UMN-TH/3720-18; CERN-TH-2018-130;
IFT-UAM/CSIC-18-58; DESY 18-086;
KCL-PH-TH/2018-22; ACFI-T18-08

Probing non-Gaussian Stochastic Gravitational Wave Backgrounds with LISA

Nicola Bartolo[a,b,c], Valerie Domcke[d], Daniel G. Figueroa[e], Juan García-Bellido[f,g], Marco Peloso [a,h], Mauro Pieroni[g], Angelo Ricciardone[i], Mairi Sakellariadou[j], Lorenzo Sorbo[k], Gianmassimo Tasinato[l]

[a] *Dipartimento di Fisica e Astronomia "G. Galilei", Università degli Studi di Padova, via Marzolo 8, I-35131, Padova, Italy*

[b] *INFN, Sezione di Padova, via Marzolo 8, I-35131, Padova, Italy*

[c] *INAF-Osservatorio Astronomico di Padova, Vicolo dell'Osservatorio 5, I-35122 Padova, Italy*

[d] *Deutsches Elektronen Synchrotron (DESY), 22607 Hamburg, Germany.*

[e] *Laboratory of Particle Physics and Cosmology Institute of Physics (LPPC), École Polytechnique Fédérale de Lausanne (EPFL), CH-1015 Lausanne, Switzerland.*

[f] *Department of Theoretical Physics, CERN, CH-1211 Genève, Switzerland*

[g] *Instituto de Física Teórica UAM/CSIC, Nicolás Cabrera 13, Universidad Autónoma de Madrid, Cantoblanco 28049 Madrid, Spain*

[h] *School of Physics and Astronomy, University of Minnesota, Minneapolis, MN 55455, USA*

[i] *Faculty of Science and Technology, University of Stavanger, 4036, Stavanger, Norway*

[j] *Theoretical Particle Physics and Cosmology Group, Department of Physics, King's College London, Strand WC2R 2LS, London, United Kingdom*

[k] *Amherst Center for Fundamental Interactions, Department of Physics, University of Massachusetts, Amherst, MA 01003, USA*

[l] *Department of Physics, Swansea University, Swansea, SA2 8PP, United Kingdom*

Abstract

The stochastic gravitational wave background (SGWB) contains a wealth of information on astrophysical and cosmological processes. A major challenge of upcoming years will be to extract the information contained in this background and to disentangle the contributions of different sources. In this paper we provide the formalism to extract, from the correlation of three signals in the Laser Interferometer Space Antenna (LISA), information about the tensor three-point function, which characterizes the non-Gaussian properties of the SGWB. Compared to the two-point function, the SGWB three-point function has a richer dependence on the gravitational wave momenta and chiralities, and a larger number of signal channels. It can be used therefore as a powerful discriminator between different models. We provide LISA's response functions to a general SGWB three-point function. As examples, we study in full detail the cases of an equilateral and squeezed SGWB bispectra, and provide the explicit form of the response functions, ready to be convoluted with any theoretical prediction of the bispectrum to obtain the observable signal. We further derive the optimal estimator to compute the signal-to-noise ratio. Our formalism covers general shapes of non-Gaussianity, and can be extended straightaway to other detector geometries. Finally, we provide a short overview of models of the early universe that can give rise to non-Gaussian SGWB.

1 Introduction

Many cosmological and astrophysical scenarios predict the existence of stochastic gravitational wave backgrounds (SGWBs) with a sufficiently large amplitude to be detectable at interferometer scales: see e.g. [1–3] for reviews. A detection of a SGWB signal would provide important information about its origin, hence it is essential to characterize its properties in detail, and to devise observables that will enable us to distinguish among different possible sources of gravitational waves (GWs).

The statistical features of a SGWB can offer various observables that can be measured with interferometers. While so far the attention has been mainly focussed on the two-point function (power spectrum) of the GW signal (see e.g. the recent review [4]), in this work we study for the first time how LISA [5] (and for this matter any other interferometer) can probe the three-point function (bispectrum) of the SGWB. A non-vanishing GW three-point function is associated with the *non-Gaussian* features of the SGWB. Some of the key ingredients of early universe models (in particular inflation and topological defects) predict that the primordial SGWB can have large non-Gaussianity, whose features can be calculated from first principles, and can be used to discriminate among different models. On the other hand, a SGWB due to a combination of a large number of uncorrelated astrophysical sources, or due to sub-horizon cosmological processes such as phase transitions or preheating, is Gaussian to a high degree, due to the central limit theorem. Thus a detection of a non-Gaussian SGWB would be a distinctive indication of a signal of cosmological origin, and the study of its properties would provide crucial information on the physics of the very early universe.

The Fourier transform of a GW three-point function defines the non-Gaussian tensor bispectrum, which depends on the frequencies of the three GWs involved, as well as on their polarization. Its scale and chirality dependence can be very rich, in contrast with the GW two-point function, whose features are very constrained by the symmetries of the underlying background geometry. This implies that a study of the GW bispectrum can lead to a large number of new observables that can be used to differentiate among different models of cosmology. So far, the physics of primordial tensor fluctuations has been mainly investigated at Cosmic Microwave Background (CMB) scales, and indeed the non-Gaussianity of primordial GWs produced in certain models of inflation have been observationally constrained by the *Planck* satellite [6].

In this work, we investigate for the first time the capabilities of LISA to test the non-Gaussian features of a SGWB via its three-point functions [1]. We do so by developing a formalism to compute the interferometer cubic response function to a non-Gaussian SGWB, connecting the GW bispectrum to the statistics of the actual signal outputs obtained from LISA (see Sections 2 and 3). We show that cubic correlators of the interferometer signal are sensitive to the properties of the GW bispectrum – its dependence on the GW wavenumber and chirality indexes – and also depends on specific features of the interferometer, like its arm configurations. Measurements of the cubic interferometer signal can distinguish among different cosmological models for a SGWB, and we show how different examples of primordial bispectra, with distinctive dependence on the momenta of the incoming GWs, lead to qualitatively distinguishable features in the interferometer cubic correlators. We also demonstrate that any measurement of the GW bispectrum at LISA is invariant under parity. Nonetheless, the analysis of LISA data can allow to extract nontrivial dependence on the correlators of the left- and right-handed

[1] Here we are interested in probing the intrinsic non-Gaussian statistics of the SGWB, and not in describing 'pop-corn-like' non-Gaussian bursts sometimes present in the unresolved stochastic background due to combining many individual sources. See [4] for a detailed review on searches for this kind of non-Gaussian signatures using the SGWB two-point function.

gravitational waves, such as the relative amplitudes of the $(\langle RRR\rangle + \langle LLL\rangle)$ and $(\langle RRL\rangle + \langle LLR\rangle)$ correlation functions.

These results allow us to build the optimal estimator for the GW bispectrum observed at LISA, generalizing to the three-point function results previously developed for studying the GW two-point function [7], see Section 4. Our final expression for the Signal-to-Noise-Ratio (SNR) is physically transparent, and we apply it to a specific scenario of primordial GW non-Gaussian signal – whose bispectrum is amplified at a specific scale – to quantitatively demonstrate the ability of LISA to measure tensor non-Gaussianity, depending on the amplitude of the GW bispectrum.

Our results demonstrate that the statistics of the GW signal measured at interferometer is sensitive to various distinctive properties of the bispectrum of primordial GWs from the early universe: Section 5 surveys existing cosmological models capable of producing large non-Gaussianity of the SGWB, analyzing the features of the corresponding bispectra, and briefly discussing prospects of detection with the LISA interferometer and with CMB experiments, in light of our findings.

Section 6 contains our conclusions, with a summary of our results and suggestions for future studies, while five appendices contain technical results used in the main text.

2 A formalism for tensor non-Gaussianity

In this section we build a formalism for describing tensor non-Gaussianity, which can be used to conveniently analyze how to probe this observable with interferometers. We consider a stochastic background of gravitational waves associated with the transverse-traceless metric perturbation $h_{ab}\,(t, \vec{x})$ of the background metric (where a, b correspond to spatial indexes, while λ denotes tensor polarization). We decompose the tensor modes as

$$\begin{aligned} h_{ab}\,(t,\,\vec{x}) &= \int d^3k\, \mathrm{e}^{-2\pi i\,\vec{k}\cdot\vec{x}} \sum_{\lambda} e_{ab,\lambda}(\hat{k}) \left[\mathrm{e}^{2\pi i\,kt}\, h_{\lambda}(\vec{k}) + \mathrm{e}^{-2\pi i\,kt}\, h^{*}_{\lambda}(-\vec{k})\right] \\ &\equiv \int d^3k\, \mathrm{e}^{-2\pi i\,\vec{k}\cdot\vec{x}} \sum_{\lambda} e_{ab,\lambda}(\hat{k})\, h_{\lambda}(t,\,\vec{k})\,, \end{aligned} \tag{1}$$

where $k \equiv |\vec{k}|$, $\hat{k}$ denotes a unit vector in the direction of the vector $\vec{k}$. In this expression, we sum over the two transverse polarizations λ of a GW, with $e_{ab,\lambda}(\hat{k})$ being the polarization operator for the polarization λ. For a more detailed discussion on the definition and construction of different polarization basis, and the properties they satisfy, we refer the reader to Appendix A.

As we require that $h_{ab}(t, \vec{x})$ is real, it must follow that

$$\sum_{\lambda} e^{*}_{ab,\lambda}(\hat{k})\, h^{*}_{\lambda}(t,\,\vec{k}) = \sum_{\lambda} e_{ab,\lambda}(-\hat{k})\, h_{\lambda}(t, -\vec{k}) \tag{2}$$

holds. This condition, however, does not fix completely the choice of the polarization tensors $e_{ab,\lambda}(\hat{k})$. Two basis for the GW polarizations are commonly employed in the literature, the $\{+,\,\times\}$ basis, and the $\{R,\,L\}$ chiral basis. In the explicit computations performed in this paper, the chiral basis is used. Furthermore, we choose chiral polarization operators that specifically satisfy $e^{*}_{ab,\lambda}(\hat{k}) = e_{ab,\lambda}(-\hat{k})$ [for chiral polarization operators that do not satisfy this property, see Appendix A]. This implies that the same property is also satisfied by the momentum space variable $h_{\lambda}(t, \vec{k})$, so that the reality of $h_{ab}(t, \vec{x})$ is ensured. Given our choice, we have

$$e^{*}_{ab,\lambda}\left(\hat{k}\right) = e_{ab,\lambda}\left(-\hat{k}\right) = e_{ab,-\lambda}\left(\hat{k}\right) \quad , \quad e^{*}_{ab,\lambda}\left(\hat{k}\right) e_{ab,\lambda'}\left(\hat{k}\right) = \delta_{\lambda\lambda'}\,. \tag{3}$$

In particular, the second equality in the first expression states that $e_{ab,R} \leftrightarrow e_{ab,L}$ under a parity transformation.

The statistical properties of the GW background are controlled by its correlation functions in Fourier space. In this work we consider the 2−point correlator $\left\langle h^2 \right\rangle$, and, more in detail, the 3−point correlator $\left\langle h^3 \right\rangle$, which is non-vanishing for a non-Gaussian SGWB. Assuming statistical isotropy, the equal-time momentum-space correlator is given by

$$\left\langle h_\lambda \left(t, \vec{k}\right) h_{\lambda'} \left(t, \vec{k}'\right) \right\rangle = \frac{P_\lambda (k)}{4\pi k^3} \delta_{\lambda\lambda'} \delta^{(3)} \left(\vec{k} + \vec{k}'\right) , \tag{4}$$

where $P_\lambda (k)$ is the power spectrum of the helicity λ, and the numerical factor at the right-hand side has been fixed imposing that the combination of eqs. (1) and (4) leads to the real space correlator

$$\langle h_{ab} (t, \vec{x}) \, h_{ab} (t, \vec{y}) \rangle = \int_0^\infty \frac{dk}{k} \sum_\lambda P_\lambda (k) \, \frac{\sin (2\pi k r)}{2\pi k r} \quad , \quad r \equiv |\vec{x} - \vec{y}| \, . \tag{5}$$

For studying the 3−point function, we use an ansatz analogous to the one used for describing the statistics of primordial scalar perturbations [8–13], see for example [14–16]. Specifically, we assume a small departure from Gaussianity, so that a tensor mode is the sum of a dominant Gaussian component, and its quadratic convolution

$$\begin{aligned} h_\lambda \left(t, \vec{k}\right) = h_{\lambda,g} \left(t, \vec{k}\right) + \sum_{\lambda',\lambda''} f_{\rm NL}^{\lambda,\lambda',\lambda''} \int d^3p \, d^3q h_{\lambda',g} (t, \vec{p}) \, h_{\lambda'',g} (t, \vec{q}) \\ \times \delta^{(3)} \left(\vec{k} - \vec{p} - \vec{q}\right) K_{\lambda\lambda'\lambda''} (-\vec{p}, -\vec{q}) \, . \end{aligned} \tag{6}$$

This ansatz is characterized by a kernel $K_{\lambda\lambda'\lambda''}$, which depends on the GW momenta and polarizations. We shall see that the kernel defines the properties of the non-Gaussian tensor bispectrum. We assume that, in general, the two different polarizations can be coupled in the convolution. Due to statistical isotropy, the kernel function depends on the magnitude of the three vectors $\vec{k}$, $\vec{p}$, $\vec{q}$ involved in the convolution,

$$\delta^{(3)} \left(\vec{k} - \vec{p} - \vec{q}\right) K_{\lambda\lambda'\lambda''} (-\vec{p}, -\vec{q}) = \delta^{(3)} \left(\vec{k} - \vec{p} - \vec{q}\right) K_{\lambda\lambda'\lambda''} (k; p, q) \, , \tag{7}$$

and it is symmetric in the last two arguments, but not in the first one, $f_{\rm NL}^{\lambda,\lambda',\lambda''} K_{\lambda\lambda'\lambda''} (k; p, q) = f_{\rm NL}^{\lambda,\lambda',\lambda''} K_{\lambda\lambda''\lambda'} (k; q, p)$. The momentum dependence of the kernel controls the so-called *shape* of the non-Gaussianity [11], namely how the bispectrum changes according to different triangular configurations in Fourier space. The simplest form of non-Gaussianity is the so called local shape, enhanced in the squeezed limit of the bispectrum, for which (assuming also that the different helicities are not mixed in the convolution) $K_{\lambda\lambda'\lambda''} (k; p, q) = \delta_{\lambda\lambda'} \delta_{\lambda\lambda''}$. More in general, we normalize $K_{\lambda\lambda'\lambda''} (k_p; k_p, k_p) = 1$ at some given pivot scale k_p, so that the size of non-Gaussianity is controlled by the nonlinear parameter $f_{\rm NL}^{\lambda,\lambda',\lambda''}$. In the concrete example of non scale-invariant Non-Gaussianity that we study in this paper, the pivot scale is chosen to be the scale at which the bispectrum is maximum, see eq. (66).

It is important to note that the mode functions appearing in the relation (6) are evaluated today. If the GW has a cosmological origin, we need to account for its evolution. It is conventional to encode this in a cosmological transfer function

$$h_\lambda (t_0, k) = \mathbf{T} (t_0, k) \, h_\lambda^{\rm pr} (k) \, , \tag{8}$$

where t_0 indicates the present time, and $h^{\rm pr}$ is the primordial value of the GW mode. For an adiabatic tensor mode produced during inflation, $h^{\rm pr}_\lambda$ is constant (time independent) at super-horizon scales. For GW produced inside the horizon after inflation, we take the value of the mode at the end of GW production. Correspondingly, eq. (6) is changed into

$$\begin{aligned}
&\mathbf{T}\left(t_0,\, k\right)\, h^{\rm pr}_\lambda(\vec{k}) = \mathbf{T}\left(t_0,\, k\right)\, h^{\rm pr}_{\lambda,g}(\vec{k}) \\
&+\sum_{\lambda',\lambda''} f_{\rm NL}^{\lambda,\lambda',\lambda''} \int d^3p d^3q \mathbf{T}\left(t_0,\, p\right)\, h^{\rm pr}_{\lambda',g}\left(\vec{p}\right)\, \mathbf{T}\left(t_0,\, q\right)\, h^{\rm pr}_{\lambda'',g}\left(\vec{q}\right) \delta^{(3)}\left(\vec{k}-\vec{p}-\vec{q}\right)\, K_{\lambda\lambda'\lambda''}\left(-\vec{p},\, -\vec{q}\right)\,.
\end{aligned} \tag{9}$$

This leads to the relation

$$f_{\rm NL}^{\lambda,\lambda',\lambda'',{\rm pr}}\, K_{\lambda\lambda'\lambda'',{\rm pr}}\left(k; p,\, q\right) \equiv \frac{\mathbf{T}\left(t_0,\, p\right)\, \mathbf{T}\left(t_0,\, q\right)}{\mathbf{T}\left(t_0,\, k\right)}\, f_{\rm NL}^{\lambda,\lambda',\lambda''}\, K_{\lambda\lambda'\lambda''}\left(k;\, p,\, q\right)\,, \tag{10}$$

between the parametrization of non-Gaussianity in terms of the primordial vs. the present day GW mode functions. [2] While the product of the last two factors at the *rhs* is more directly related to what we measure, the *lhs* is more immediately connected to the theory that provides the origin of the non-Gaussianity.

From the ansatz (6) we obtain the equal-time three-point function, to linear order in the nonlinear parameters, as

$$\left\langle h_{\lambda_1}\left(t,\, \vec{k}_1\right) h_{\lambda_2}\left(t,\, \vec{k}_2\right) h_{\lambda_3}\left(t,\, \vec{k}_3\right)\right\rangle = \delta^{(3)}\left(\vec{k}+\vec{k}_2+\vec{k}_3\right) \mathcal{B}_{\lambda_1,\lambda_2,\lambda_3}\left(k_1,k_2,k_3\right)\,, \tag{11}$$

with

$$\begin{aligned}
\mathcal{B}_{\lambda_1,\lambda_2,\lambda_3}\left(k_1,k_2,k_3\right) \;=\; & \frac{f_{\rm NL}^{\lambda_1,\lambda_2,\lambda_3}}{8\pi^2}\, K_{\lambda_1;\lambda_2,\lambda_3}\left(k_1;k_2,k_3\right) \frac{P_{\lambda_2}\left(k_2\right)}{k_2^3}\, \frac{P_{\lambda_3}\left(k_3\right)}{k_3^3} \\
& + \frac{f_{\rm NL}^{\lambda_2,\lambda_1,\lambda_3}}{8\pi^2}\, K_{\lambda_2;\lambda_1,\lambda_3}\left(k_2;k_1,k_3\right) \frac{P_{\lambda_1}\left(k_1\right)}{k_1^3}\, \frac{P_{\lambda_3}\left(k_3\right)}{k_3^3} \\
& + \frac{f_{\rm NL}^{\lambda_3,\lambda_1,\lambda_2}}{8\pi^2}\, K_{\lambda_3;\lambda_1,\lambda_2}\left(k_3;k_1,k_2\right) \frac{P_{\lambda_1}\left(k_1\right)}{k_1^3}\, \frac{P_{\lambda_2}\left(k_2\right)}{k_2^3}\,.
\end{aligned} \tag{12}$$

This expression for the bispectrum can describe the different shapes of non-Gaussianity, and the dependence on chirality. The expression for the tensor three-point function (11) evaluated at non-equal times, which will be used in Section 4, is discussed in Appendix B.

3 LISA signal and response functions

Our aim in this Section is to build the tools to study the primordial tensor three-point functions with LISA: we connect the theoretical results of the previous section with the actual LISA design. We analyze how the signal cubic correlator can be used to probe the tensor bispectrum described in Section 2, deriving for the first time the interferometer cubic response function to tensor non-Gaussianity. As

[2] To be precise, both sides in this relation are multiplied by $\delta^{(3)}(\vec{k}+\vec{p}+\vec{q})$. Eq. (10) indicates in an unambiguous way how the nonlinear parameter $f_{\rm NL}$ and the kernel function K should be independently rescaled, once we demand that both the present day and the primordial kernel function are normalized to $K_{\lambda\lambda'\lambda''}\left(k_p;\, k_p,\, k_p\right) = K_{\lambda\lambda'\lambda'',{\rm pr}}\left(k_p;\, k_p,\, k_p\right) = 1$.

we shall see, the interferometer response function is sensitive to the shape and polarization dependence of the primordial tensor bispectrum.

We first analyze how a SGWB influences the time a photon takes for traveling along a single arm of an interferometer. We then study the signal measured at LISA. We follow the derivation done in [4,17] based on the frequency basis (C1) that we introduce in the appendix C, but reformulated in the basis (1).

3.1 Single arm of an interferometer

We consider an interferometer arm at rest, with mass 1 and mass 2 at the two ends. Mass 1 and mass 2 are located, respectively, at $\vec{x}_1$ and at $\vec{x}_2 = \vec{x}_1 + L\,\hat{l}_{12}$, where L is the length of the arm, and $\hat{l}_{12}$ the unit vector in the direction from mass 1 to mass 2. The change in the light-travel time for a photon emitted at mass 1 at the time t_1 and arriving at mass 2, due to a passing gravitational wave h_{ab} is given by

$$\Delta T\left(t_1\right) = \frac{1}{2}\hat{l}^a_{12}\hat{l}^b_{12}\int_0^L ds\, h_{ab}\left(t_1+s,\,\vec{x}_1+s\,\hat{l}_{12}\right)\,. \tag{13}$$

Inserting the decomposition (1) and performing the integral, we find

$$\Delta T\left(t_1\right) = L\int d^3k\, \mathrm{e}^{-2\pi i\vec{k}\cdot\vec{x}_1}\sum_\lambda e_{ab,\lambda}\left(\hat{k}\right)\frac{\hat{l}^a_{12}\hat{l}^b_{12}}{2}\Bigg[\mathrm{e}^{2\pi i k t_1}\hat{h}_\lambda\left(\vec{k}\right)\,\mathcal{M}\left(\hat{l}_{12}\cdot\hat{k},\,k\right) + \mathrm{e}^{-2\pi i k t_1}\hat{h}^*_\lambda\left(-\vec{k}\right)\,\mathcal{M}^*\left(-\hat{l}_{12}\cdot\hat{k},\,k\right)\Bigg]\,, \tag{14}$$

with

$$\mathcal{M}\left(\hat{l}_{12}\cdot\hat{n},\,k\right) \equiv \mathrm{e}^{\pi i k L\left[1-\hat{n}\cdot\hat{l}_{12}\right]}\,\frac{\sin\left(\pi k L\left[1-\hat{n}\cdot\hat{l}_{12}\right]\right)}{\pi k\left[1-\hat{n}\cdot\hat{l}_{12}\right]}\,, \tag{15}$$

where $\hat{n}$ is the direction of propagation of the wave. Let us consider now the signal $s_{12}\left(t,\,\vec{x}_1\right)$, measured at time t by a detector of mass 1 located at $\vec{x}_1$, as the sum of the change in the light-travel time for a photon emitted at mass 1 (at the time $t-2L$), arriving to mass 2 (at the time $t-L$), and then coming back to mass 1, i.e.,

$$s_{12}\left(t\right) = \Delta T_{12}\left(t-2L\right) + \Delta T_{21}\left(t-L\right) + n_1\left(t\right)\,, \tag{16}$$

where $n_1\left(t\right) = n_1\left(t,\vec{x}_1\right)$ is the noise measured by the detector. Using eq. (14) we obtain

$$s_{12}\left(t,\,\vec{x}_1\right) - n_1\left(t,\,\vec{x}_1\right) = L\int d^3k\,\mathrm{e}^{-2\pi i\vec{k}\cdot\vec{x}_1}\sum_\lambda \mathcal{G}_\lambda\left(\hat{k},\hat{l}_{12}\right)\,h_\lambda\left(t-L,\,\vec{k}\right)\,\mathcal{T}\left(kL,\,\hat{k}\cdot\hat{l}_{12}\right)\,, \tag{17}$$

where the detector transfer function[3] is

$$\mathcal{T}\left(kL,\,\hat{k}\cdot\hat{l}_{12}\right) \equiv \mathrm{e}^{-\pi i k L\left[1+\hat{k}\cdot\hat{l}_{12}\right]}\,\frac{\sin\left(\pi k L\left[1-\hat{k}\cdot\hat{l}_{12}\right]\right)}{\pi k L\left[1-\hat{k}\cdot\hat{l}_{12}\right]} + \mathrm{e}^{\pi i k L\left[1-\hat{k}\cdot\hat{l}_{12}\right]}\,\frac{\sin\left(\pi k L\left[1+\hat{k}\cdot\hat{l}_{12}\right]\right)}{\pi k L\left[1+\hat{k}\cdot\hat{l}_{12}\right]}\,, \tag{18}$$

[3]The detector transfer function $\mathcal{T}$ encodes the response of the detector to a gravitational wave, and should not be confused with the cosmological transfer function introduced in eq. (8).

and we have also introduced the combination

$$\mathcal{G}_\lambda\left(\hat{k},\hat{l}_{12}\right)\equiv e_{ab,\lambda}\left(\hat{k}\right)\frac{\hat{l}^a_{12}\hat{l}^b_{12}}{2}\,. \tag{19}$$

Using (4), we obtain the 2−point correlation function of the signal

$$\left\langle s^2_{12}\left(t,\,\vec{x}_1\right)\right\rangle-\left\langle n^2_1\left(t,\,\vec{x}_1\right)\right\rangle=\frac{L^2}{4\pi}\int\frac{d^3k}{k^3}\sum_\lambda P_\lambda\left(k\right)\left|\mathcal{G}_\lambda\left(\hat{k},\hat{l}_{12}\right)\right|^2\left|\mathcal{T}\left(kL,\,\hat{k}\cdot\hat{l}_{12}\right)\right|^2\,, \tag{20}$$

as well as the 3−point correlation function

$$\begin{aligned}\left\langle s^3_{12}\left(t,\,\vec{x}_1\right)\right\rangle-\left\langle n^3_1\left(t,\,\vec{x}_1\right)\right\rangle=L^3\int d^3k_1\int d^3k_2\int d^3k_3\,\delta^{(3)}\left(\vec{k}_1+\vec{k}_2+\vec{k}_3\right)\mathcal{B}_{\lambda_1\lambda_2\lambda_3}\left(k_1,k_2,k_3\right)\\ \times\sum_{\lambda_1,\lambda_2,\lambda_3}\mathcal{G}_{\lambda_1}\left(\hat{k}_1,\,\hat{l}_{12}\right)\mathcal{G}_{\lambda_2}\left(\hat{k}_2,\,\hat{l}_{12}\right)\mathcal{G}_{\lambda_3}\left(\hat{k}_3,\,\hat{l}_{12}\right)\\ \times\mathcal{T}\left(k_1L,\,\hat{k}_1\cdot\hat{l}_{12}\right)\mathcal{T}\left(k_2L,\,\hat{k}_2\cdot\hat{l}_{12}\right)\mathcal{T}\left(k_3L,\,\hat{k}_3\cdot\hat{l}_{12}\right)\,,\end{aligned} \tag{21}$$

where we have assumed that signal and noise are uncorrelated (i.e., $\langle s\,n\rangle=\langle s\,n^2\rangle=\langle s^2n\rangle=0$).

3.2 Quadratic and cubic signal correlation functions at LISA

Equation (17) describes the signal generated in a single arm of an interferometer. From this result we can construct the response functions of the full instrument, where the phase measurements in the individual arms are combined to minimize the instrumental noise (see e.g. [18]). Combining two arms of the equilateral triangular LISA configuration with a common mass at $\vec{x}_1$ yields a Michelson interferometer:

$$s_X(t,\vec{x}_1)-n_X(t,\vec{x}_1)=\Delta T_{12}(t-2L)+\Delta T_{21}(t-L)-\Delta T_{13}(t-2L)-\Delta T_{31}(t-L)\,. \tag{22}$$

Cyclic permutation of the endpoints $\vec{x}_1,\vec{x}_2,\vec{x}_3$ results in a total of three Michelson interferometers, which we label X, Y and Z. From these, the standard LISA output channels A, E and T are constructed as [18]

$$s_A(t)=\frac{1}{3}(2s_X(t)-s_Y(t)-s_Z(t))\,, \tag{23}$$

$$s_E(t)=\frac{1}{\sqrt{3}}(s_Z(t)-s_Y(t))\,, \tag{24}$$

$$s_T(t)=\frac{1}{3}(s_X(t)+s_Y(t)+s_Z(t))\quad\text{(null channel)}\,. \tag{25}$$

These signals can then be expressed as a linear combination of the single arm signals,

$$s_O(t)=\sum_{i,j}c^O_{ij}\,s_{ij}(t)\,,\quad O\in\{A,E,T\}\,, \tag{26}$$

where $i,j=1,2,3$ label the test masses and c^O_{ij} are constant coefficients which can be read from eqs. (22)-(25). Introducing

$$\mathcal{I}^{ij}_\lambda(\vec{k})\equiv e^{-2\pi i\vec{k}\cdot\vec{x}_i}\,\mathcal{G}_\lambda(\hat{k},\hat{l}_{ij})\,\mathcal{T}\left(kL,\,\hat{k}\cdot\hat{l}_{ij}\right)\,, \tag{27}$$

the arm signal eq. (17) can be compactly written as

$$s_{12}(t,\vec{x}_1) - n(t,\vec{x}_1) = L \int d^3k \sum_\lambda \mathcal{I}^{12}_\lambda(\vec{k})\; h_\lambda(t-L,\vec{k})\,. \tag{28}$$

Correspondingly,

$$s_O(t) - n_O(t) = L \int d^3k \sum_{i,j} c^O_{ij}\, \mathcal{I}^{ij}_\lambda(\vec{k})\; h_\lambda(t-L,\vec{k})\,, \tag{29}$$

with c^O_{ij} the same coefficients as in eq. (26).

We now have the tools to study the two-point and three-point correlation functions for the signal, and analyze how they depend on the statistical properties of the SGWB, namely its power spectrum and bispectrum as described in Section 2. We derive the quadratic and cubic interferometer response functions, and discuss how the interferometer measurements allow to probe properties of the primordial tensor non-Gaussianity.

3.2.1 The quadratic interferometer response function

The quadratic auto-correlation of the interferometer signal reads

$$\langle s^2_O(t)\rangle - \langle n^2_O(t)\rangle = \frac{L^2}{4\pi}\int \frac{dk}{k}\sum_\lambda P_\lambda(k) \int d\hat{k}\left(c^O_{ij}\,\mathcal{I}^{ij}_\lambda(\vec{k})\right)\left(c^O_{lm}\,\mathcal{I}^{lm}_\lambda(-\vec{k})\right) \tag{30}$$

$$= L^2 \int \frac{dk}{k}\sum_\lambda P_\lambda(k) \underbrace{\frac{1}{4\pi}\,2\int_{\theta<\frac{\pi}{2}} d\hat{k}\left|c^O_{ij}\,\mathcal{I}^{ij}_\lambda(\vec{k})\right|^2}_{\equiv \mathcal{R}^{OO}_\lambda(k)}, \tag{31}$$

where we have inserted eq. (4) and used the fact that $\mathcal{I}^{ij}_\lambda(-\vec{k}) = (\mathcal{I}^{ij}_\lambda(\vec{k}))^*$ [recall that this property is specific to our choice of polarization operators eq. (3)] to halve the domain of the momentum integration.

The quantity $\mathcal{R}^{OO}_\lambda(k)$ gives the (scale-dependent) detector response function to the GW of polarization h_λ for the 2-point correlation function of the channel O. This is obtained after integrating $\left|c^O_{ij}\,\mathcal{I}^{ij}_\lambda(\vec{k})\right|^2$ over all the directions $\hat{k}$ of the incoming GW.

The angular-dependent integrand is shown in Fig. 1, for the specific choice $k = 0.1/L$ of the GW wavenumber and for the two channels A (left panel) and E (right panel), respectively. We disregard the T channel, as its sensitivity to the GW background is well below that of the A and E channels [18] (we have verified that this is the case also for the 3−point functions that we study below). We use standard spherical coordinates, where $\theta \in [0,\,\pi]$ is the polar angle, and $\phi \in [0,\,2\pi]$ is the azimuthal angle. For definiteness, we set the detector in the xz-plane, with the three masses, respectively at the $\{x,\,z\}$ locations given by $\{0,\,0\}$, $\{0,\,L\}$, and $\left\{\frac{\sqrt{3}}{2}L,\,\frac{L}{2}\right\}$. As expected GWs arriving from the perpendicular direction to the detector (the y axis, characterized by $\theta = \frac{\pi}{2}$ and $\phi = \frac{\pi}{2},\,\frac{3\pi}{2}$) are those that provide the largest contribution to the detector two-point function. For equal length interferometer arms the cross response function $\mathcal{R}^{AE}$ vanishes [18].

In Fig. 2 we show the detector response function (after integrating over the GW directions). The same result is obtained for both polarizations (we discuss this below) and in the two channels A and

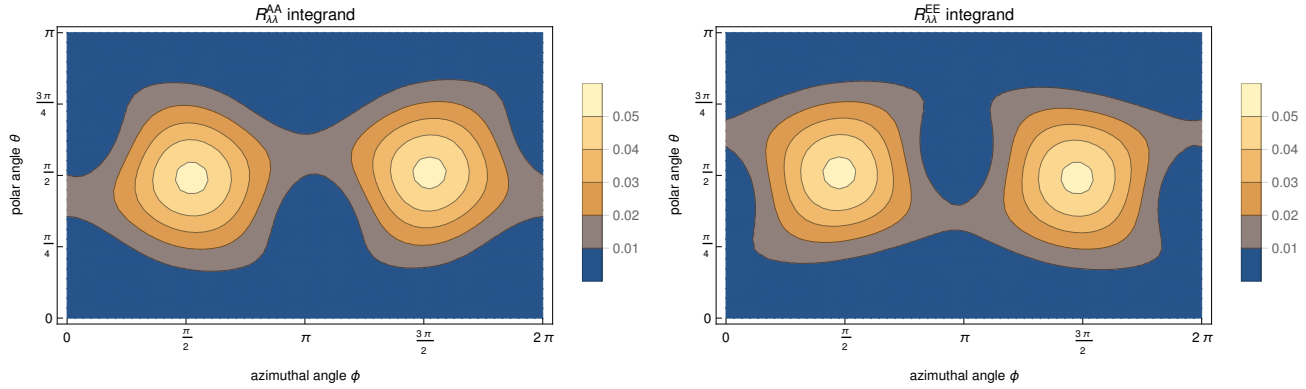

Figure 1: *Directional dependence of the integrand for the response functions* $\mathcal{R}^{AA}_{R}(k)$ *(left panel) and* $\mathcal{R}^{EE}_{R}(k)$*. The wavenumber* k *of the GW has been chosen to be* $0.1/L$*. The response functions for the left-handed polarizations are obtained by a parity transformation about the plane of the detector (the* xz *plane, in our choice), which for our case corresponds to* $\phi \to -\phi$ *(as discussed in the text).*

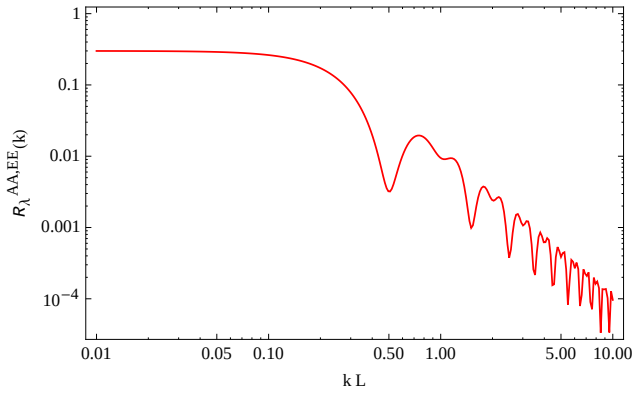

Figure 2: *Integrated response function* $\mathcal{R}^{OO}_{\lambda}(k)$ *for* $O = \{A, E\}$ *and* $\lambda = \{L, R\}$.

E. The response function is nearly constant up to $k \sim 0.2/L$, and it then strongly decreases with k. By Taylor expanding the relations (27) in the limit of small k, we have the analytic result

$$\mathcal{R}^{AA}_{\lambda}(k) = \mathcal{R}^{EE}_{\lambda}(k) = \frac{3}{10} - \frac{169}{1680}\left(\frac{k}{k_*}\right)^2 + \mathrm{O}\left(\frac{k^4}{k_*^4}\right) \quad , \quad k_* \equiv \frac{1}{2\pi L} \, . \tag{32}$$

This agrees with the first of eqs. (18) in [19].

3.2.2 The cubic interferometer response function

We now derive for the first time the interferometer cubic response function, starting from the expression

$$\begin{aligned} &\langle s_{O_1}(t) s_{O_2}(t) s_{O_3}(t)\rangle - \langle n_{O_1}(t) n_{O_2}(t) n_{O_3}(t)\rangle \\ &\quad = \int d^3k_1 \int d^3k_2 \int d^3k_3 \sum_{\lambda_1,\lambda_2,\lambda_3} \mathcal{B}_{\lambda_1\lambda_2\lambda_3}(k_1,k_2,k_3)\, \delta^{(3)}(\vec{k}_1+\vec{k}_2+\vec{k}_3)\, \Pi_{l=1}^{3}\left(c_{ij}^{O_l}\, \mathcal{I}^{ij}_{\lambda_l}(\vec{k}_l)\right) \, . \end{aligned} \tag{33}$$

The computation is conceptually similar to the one done for the two-point response function, with the complication of various angular integrations: the task is to find the most convenient way to perform the integrals and obtain an expression for the response function in terms of the momenta of the incoming GW waves.

We use the Dirac $\delta-$function to perform three of the angular integrations. We are left with six integrations to do: three over the magnitudes of the momenta, and three over angles. The angles parameterize respectively the direction of $\hat{k}_1$, and the rotation of $\hat{k}_2$ about $\hat{k}_1$, keeping fixed the angle θ_{12} between the two vectors. The latter angle can be expressed using the $\delta-$function, since

$$\vec{k}_3 = -\vec{k}_1 - \vec{k}_2 \quad \Rightarrow \quad \cos\,\theta_{12} = \frac{k_3^2 - k_1^2 - k_2^2}{2k_1k_2} \, . \tag{34}$$

The specific algorithm that we employ to compute these integrals is the following. We consider an auxiliary coordinate system in which $\hat{k}_1$ is oriented along the $z-$ axis, and $\hat{k}_2$ is initially in the xz plane, at an angle θ_{12} with the $z-$axis (and with positive $x-$component), and it is then rotated by the angle ϕ_2 about the $z-$axis. In this auxiliary system, $\hat{k}_1$ and $\hat{k}_2$ coincide, respectively, with the unit vectors

$$\hat{v}_1 = \begin{pmatrix} 0 \\ 0 \\ 1 \end{pmatrix} \quad , \quad \hat{v}_2 = \begin{pmatrix} \sqrt{1-\left(\frac{k_3^2-k_1^2-k_2^2}{2k_1k_2}\right)^2}\,\cos\phi_2 \\ \sqrt{1-\left(\frac{k_3^2-k_1^2-k_2^2}{2k_1k_2}\right)^2}\,\sin\phi_2 \\ \frac{k_3^2-k_1^2-k_2^2}{2k_1k_2} \end{pmatrix} \, . \tag{35}$$

We then move to the actual coordinate system by rotating $\hat{k}_1$ and $\hat{k}_2$ through the same rotation matrix

$$R_1 = \begin{pmatrix} \cos\theta_1\,\cos\phi_1 & -\sin\phi_1 & \sin\theta_1\,\cos\phi_1 \\ \cos\theta_1\,\sin\phi_1 & \cos\phi_1 & \sin\theta_1\,\sin\phi_1 \\ -\sin\theta_1 & 0 & \cos\theta_1 \end{pmatrix} \, , \tag{36}$$

and finally the third vector is given by $\vec{k}_3 = -\vec{k}_1 - \vec{k}_2$. By working out the Jacobian of the transformation, we obtain

$$\langle s_{O_1} s_{O_2} s_{O_3}\rangle = L^3 \int \frac{dk_1}{k_1} \int \frac{dk_2}{k_2} \int \frac{dk_3}{k_3} \sum_{\lambda_1\lambda_2\lambda_3} k_1^2\, k_2^2\, k_3^2\, \mathcal{B}_{\lambda_1\lambda_2\lambda_3}(k_1,\,k_2,\,k_3)\; \mathcal{R}^{O_1O_2O_3}_{\lambda_1\lambda_2\lambda_3}(k_1,\,k_2,\,k_3) \, ,$$

(37)

with

$$\mathcal{R}^{O_1O_2O_3}_{\lambda_1\lambda_2\lambda_3}(k_1,\,k_2,\,k_3) = \int_0^{\pi} d\theta_1 \int_0^{2\pi} d\phi_1 \int_0^{2\pi} d\phi_2 \sin\theta_1 \,\Pi_{l=1}^{3} c_{ij}^{O_l}\,\mathcal{I}^{ij}_{\lambda_l}\left(\vec{k}_l\right)\Big|_{\vec{k}_1=k_1\,R_1\,\hat{v}_1,\,\vec{k}_2=k_2\,R_1\,\hat{v}_2\,,\,\vec{k}_3=-\vec{k}_1-\vec{k}_2}\,. \tag{38}$$

Also in this case, a parity transformation ($\vec{k}_i \to -\vec{k}_i$, corresponding to $\theta_1 \to \pi - \theta_1$, $\phi_1 \to \pi + \phi_1$, $\phi_2 \to \pi - \phi_2$) sends the integral into its complex conjugate, ensuring that the response function is a real number [again, this is a consequence of our choice of polarization operators eq. (3)]. Interestingly, we find that the different A and E channels have non-vanishing cross-correlations in the three-point functions. Moreover, the response function differs for different GW polarizations. We can therefore (at least in principle) perform several independent measurement of the GW bispectrum with LISA.

Let us emphasize that the fact that our 3-pt response function is real applies because of the choice of polarization operators in eq. (3), which are built from the canonical basis given e.g. in eq. (A3), presented in Appendix A. In such appendix we actually derive the transformation rule of the polarization operators when they are rotated by an angle α around each vector $\vec{k}$. We conclude that in general the 3-pt response functions are complex, depending on the choice of α (the 2-pt response function, however, is always real). For instance, for $\alpha = 0$ or $\alpha = \pi$, we have that all 3-pt response functions are real, whereas for $\alpha = \pi/6$ the response functions $\mathcal{R}_{RRR}, \mathcal{R}_{LLL}$ are still real, whereas $\mathcal{R}_{LRR}, \mathcal{R}_{RLL}$ become complex. The condition to be purely real, purely imaginary, or simply complex, depends on the choice of the basis depending on α, see Appendix A and in particular eqs. (A16)-(A19). Of course, the final signal in the GW detector does not depend on the arbitrary choice of the vector basis. The left hand side of eq. (37) is the same no matter what the choice of the angle α. However, depending on α, one must modify our expressions for the response functions by the phases indicated in eqs. (A16)-(A19), and at the same time correct the tensor bispectra $\mathcal{B}_{\lambda\lambda'\lambda''}$ by exactly the opposite phases, so that at the end the physical signal eq. (37) remains invariant. In order to use our formalism, special care must be put into what vector basis is being used in the computation of the tensor bispectrum, and hence what properties of the polarization operators and response functions hold. See Appendix A for further details.

We evaluate now the response function for two cases:

– *An equilateral configuration.* Let us start from the case for which $k_1 = k_2 = k_3 \equiv k$, which is defined as equilateral configuration. In the left panel of Fig. 3 we show the response functions $\mathcal{R}^{OO'O''}_{RRR}(k)$ for the various combinations of channels O, O', O''. The right panel of Fig. 3 shows instead the response functions $\mathcal{R}^{OO'O''}_{RRL}(k)$. As we discuss in the next subsection, the response functions are invariant under parity, and we find that $\mathcal{R}^{OO'O''}_{RRR} = \mathcal{R}^{OO'O''}_{LLL}$, and that $\mathcal{R}^{OO'O''}_{RRL} = \mathcal{R}^{OO'O''}_{RLL}$. Therefore, the response functions shown in Fig. 3 show all the possible independent combinations of the A and E channels.

– *A squeezed isosceles configuration.* Let us now study the response functions for the isosceles squeezed case, $k_3 \ll k_1 = k_2$. In this case, eqs. (35) and (36) give

$$\hat{v}_2 = -\hat{v}_1 - \frac{k_3}{k_1}\,\hat{v}_3 + \mathcal{O}\left(\frac{k_3^2}{k_1^2}\right) \quad , \quad \hat{v}_3 \equiv -\begin{pmatrix}\cos\phi_2\\ \sin\phi_2\\ 0\end{pmatrix} \quad \Rightarrow \quad \hat{k}_3 = R_1\,\hat{v}_3\left[1 + \mathcal{O}\left(\frac{k_3}{k_1}\right)\right], \tag{39}$$

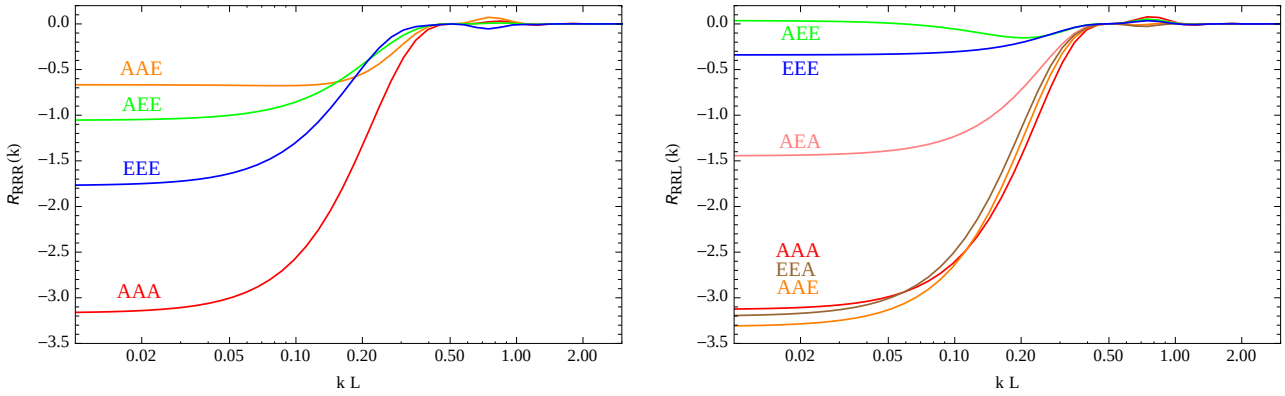

Figure 3: *Integrated response function* $\mathcal{R}^{OO'O''}_{RRR} = \mathcal{R}^{OO'O''}_{LLL}$ *(left panel) and* $\mathcal{R}^{OO'O''}_{RRL} = \mathcal{R}^{OO'O''}_{RLL}$ *(right panel) for the A and E channels (both self- and cross-correlations) for the case of an exact equilateral bispectrum (of wavenumber* k*). The label next to each curve indicates the choice of* $OO'O''$ *corresponding to that curve.*

and therefore

$$\mathcal{I}^{ij}_{\lambda}\left(\vec{k}_3\right) = e_{ab,\lambda}\left(\hat{k}_3\right)\, \hat{l}^a_{ij}\, \hat{l}^b_{ij} + \mathcal{O}\left(\frac{k_3}{k_1}\right) . \tag{40}$$

To leading order, the response function becomes

$$\begin{aligned}&\mathcal{R}^{O_1O_2O_3}_{\lambda_1\lambda_2\lambda_3}\left(k_1,\, k_1,\, k_3 \ll k_1\right)\\ &\quad\simeq \int_0^{\pi} d\theta_1\, \sin\theta_1 \int_0^{2\pi} d\phi_1\, F^{O_3}\left(\theta_1,\, \phi_1\right)\, \left[c^{O_1}_{ij}\, \mathcal{I}^{ij}_{\lambda_1}\left(k_1 R_1 \hat{v}_1\right)\right]\, \left[c^{O_2}_{ij}\, \mathcal{I}^{ij}_{\lambda_2}\left(-k_1 R_1 \hat{v}_1\right)\right] ,\end{aligned} \tag{41}$$

where we have introduced the quantities

$$F^{O}\left(\theta_1,\, \phi_1\right) \;\equiv\; c^{O}_{ij}\, \hat{l}^a_{ij} \hat{l}^b_{ij} \int_0^{2\pi} d\phi_2\, e_{ab,\lambda}\left(R_1 \hat{v}_3\right) . \tag{42}$$

Namely, the isosceles squeezed three-point response function reduces to an integration over angles of the same quantities characterizing a two-point response function, modulated by the angular function $F^{O}\left(\theta_1,\, \phi_1\right)$, depending on the orientation of the long mode with respect to the signal trajectory. This fact resembles the consistency relation for the squeezed limit of the bispectrum of adiabatic inflationary fluctuations, first discussed in [12]. Long wavelength adiabatic modes do not directly affect short wavelength ones, but instead can be thought as contributing to the background geometry: hence the squeezed limit of three-point functions quantifies how two-point functions get modulated by a background which includes the long mode.

Due to our choice $e_{ab,\lambda}\left(\hat{k}\right) = e_{ab,-\lambda}\left(-\hat{k}\right) = e^{*}_{ab,\lambda}\left(-\hat{k}\right)$, and since $R_1\hat{v}_3$ changes sign when $\phi_2 \to \phi_2 + \pi$, the functions $F^{O}\left(\theta_1,\, \phi_1\right)$ are real, and $\lambda-$independent. The integral (42) can be performed analytically, leading to

$$F^{A}_{\lambda_3}\left(\theta_1,\, \phi_1\right) \;=\; -\frac{3\pi}{128}\left\{12\left[3+\cos\left(2\theta_1\right)\right] + \frac{\cos\left(2\phi_1\right)}{\sin^2\theta_1}\left[45 + 20\cos\left(2\theta_1\right) - \cos\left(4\theta_1\right) - 64\,\left|\cos\theta_1\right|\right]\right\}$$

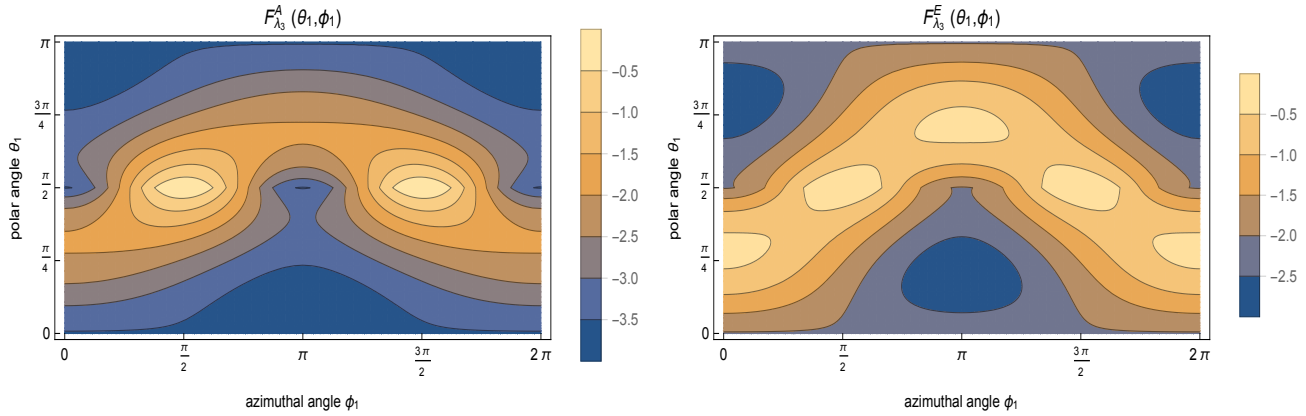

Figure 4: *Directional dependence of the integrand (41) for the response functions* $F^A_{\lambda_3}$ *(left panel) and* $F^E_{\lambda_3}$ *(right panel).*

$$
\begin{aligned}
& + \frac{\sqrt{3}\pi}{8} \sin(2\theta_1) \cos(\phi_1) \ , \\
F^E_{\lambda_3}(\theta_1,\, \phi_1) \;&=\; -\frac{\sqrt{3}\pi}{128} \left\{ 12\,[3 + \cos(2\theta_1)] + \frac{\cos(2\phi_1)}{\sin^2\theta_1}\,[45 + 20\cos(2\theta_1) - \cos(4\theta_1) - 64\,|\cos\theta_1|] \right\} \\
& + \frac{3\pi}{8} \sin(2\theta_1) \cos(\phi_1) \ , \\
F^T_{\lambda_3}(\theta_1,\, \phi_1) \;&=\; 0\,. \qquad (43)
\end{aligned}
$$

We have plotted in Fig. 4 the directional dependence of the integrand (41) for the two channels A and E.

Since the functions $F^O(\theta_1,\, \phi_1)$ are $\lambda-$independent, both GW helicities give the same response function in the isosceles squeezed limit. Using also the mirror symmetry discussed in the next subsection (namely, the response function is invariant when we change the helicities of all modes), we can see that 12 independent configuration exists, 6 having the squeezed mode measured from the A channel, and 6 from the E channel. The various independent combinations are shown in Fig. 5.

3.2.3 Three-point response function physical properties under parity

The properties of the interferometer cubic response function can be used to characterized the non-Gaussian SGWB. Tensor non-Gaussianity is described by the tensor bispectrum discussed in Section 2, and different models predict different shapes and polarization dependencies for the amplitude of the bispectrum (see Section 5 for a detailed discussion). Since we find different expressions for three-point response function depending on the momenta and on the polarization indexes, three-point functions of inteferometer signals can distinguish among different possible sources of SGWBs.

On the other hand, an additional feature that can characterize the tensor bispectrum is its behaviour under a parity transformation. Certain models of early Universe cosmology (see Section 5), predict that tensor bispectra violate parity, and the value of the bispectrum components are not invariant under a parity transformation. We now show that LISA – and any planar interferometer –

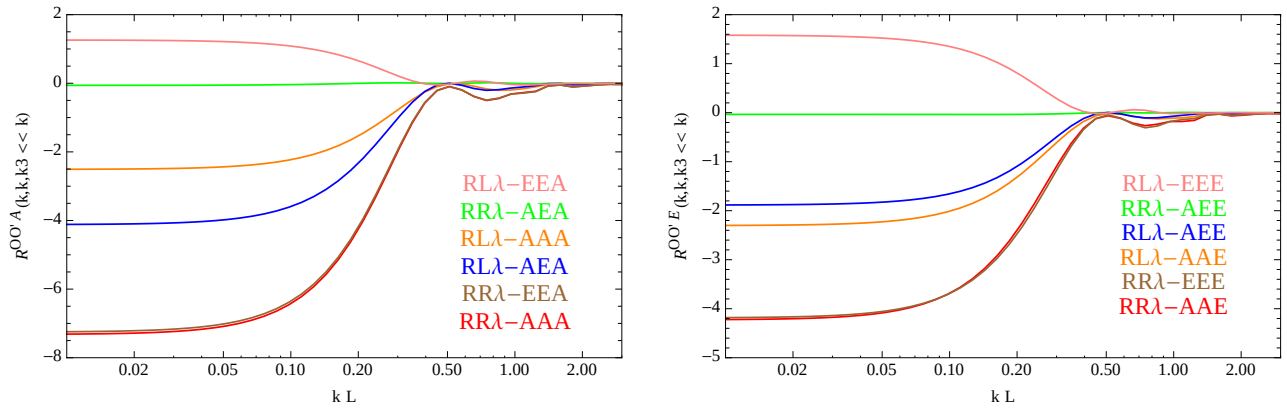

Figure 5: *Integrated response function* $\mathcal{R}^{OO'O''}_{\lambda\lambda'\lambda''}(k_1, k_2, k_3)$ *for an isosceles squeezed bispectrum,* $k_3 \ll k_1 = k_2$*, with the long mode measured from the A (left panel) and E (right panel) channel. To leading order in* k_3/k_1*, identical response functions are obtained for both helicities of the long mode.*

cannot distinguish among components of the bispectrum that differ only by a parity transformation, and consequently cannot detect parity breaking effects. Reference [7] noted that the LISA response function for the two-point function is the same for the left and right polarizations of the GW, namely $\mathcal{R}^{OO}_{\lambda} = \mathcal{R}^{OO}_{-\lambda}$, due to a mirror symmetry across the plane of the interferometer. As we show now, this result can be readily extended also to the three-point function, implying the equalities $\mathcal{R}_{RRR} = \mathcal{R}_{LLL}$ and $\mathcal{R}_{RRL} = \mathcal{R}_{LLR}$. To understand this, consider a triangular configuration of satellites on the xz plane. The mirror symmetry then corresponds to changing the y component of a vector. We would like to understand what this implies for the factor $\mathcal{I}$, defined in eq. (27), that controls the response function. Denoting by $V_{\parallel}$ and by $V_{\perp}$ the component of a vector V, respectively, inside and perpendicular to xz plane, we note that the GW momentum, and the basis vectors $\hat{u}$ and $\hat{v}$ introduced in Section 2, change as

$$\begin{aligned} &\hat{k}_{\parallel} \Rightarrow \hat{k}_{\parallel} \quad , \quad \hat{k}_{\perp} \Rightarrow -\hat{k}_{\perp} \, , \\ &\hat{u}_{\parallel} \Rightarrow -\hat{u}_{\parallel} \quad , \quad \hat{u}_{\perp} \Rightarrow \hat{u}_{\perp} \, , \\ &\hat{v}_{\parallel} \Rightarrow \hat{v}_{\parallel} \quad , \quad \hat{v}_{\perp} \Rightarrow -\hat{v}_{\perp} \, . \end{aligned} \tag{44}$$

As the vectors $\vec{l}_{ij}$ (expressing the displacements between the test masses) lie in the plane of the instrument, only the parallel components contribute to the contractions $\mathcal{G}_{\lambda}\left(\hat{k}, \hat{l}\right)$ [defined in eq. (19)]. Due to this, and thanks to the properties of (44), we see that $\mathcal{G}_{\lambda} \to \mathcal{G}_{-\lambda}$ under this mirror transformation. On the other hand, the transfer function $\mathcal{T}$ and the phase entering in eq. (27) are invariant under this transformation. This implies that $\mathcal{I}^{ij}_{\lambda}\left(k_{\parallel}, k_{\perp}\right) = \mathcal{I}^{ij}_{-\lambda}\left(k_{\parallel}, -k_{\perp}\right)$. The same property holds for the linear combinations $c^0_{ij}\,\mathcal{I}^{ij}_{\lambda}$. These combinations form the response functions, which, therefore,

satisfy [4]

$$\mathcal{R}_{\lambda}^{OO'}\left(k_{\parallel},\, k_{\perp}\right) = \mathcal{R}_{-\lambda}^{OO'}\left(k_{\parallel},\, -k_{\perp}\right) \quad , \quad \mathcal{R}_{\lambda\lambda'\lambda''}^{OO'O''}\left(k_{i,\parallel},\, k_{i,\perp}\right) = \mathcal{R}_{-\lambda-\lambda'-\lambda''}^{OO'O''}\left(k_{i,\parallel},\, -k_{i,\perp}\right) \, . \tag{45}$$

After integrating over the angles, this implies the equalities $\mathcal{R}_{RR} = \mathcal{R}_{LL}$ for the two-point function found in [7], as well as the equalities $\mathcal{R}_{RRR} = \mathcal{R}_{LLL}$ and $\mathcal{R}_{RRL} = \mathcal{R}_{RLL}$ for the three-point function. This implies that parity violation in the tensor bispectrum can not be detected using a planar interferometer, like LISA.

4 The optimal signal-to-noise ratio

In this section we construct a frequency-dependent estimator of the stochastic gravitational wave bispectrum. Our procedure extends to the case of a signal three-point function the arguments developed in [7] to estimate the optimal signal-to-noise ratio in the gravitational wave power spectrum.

4.1 The signal in frequency space

Since our goal is to generate a frequency-dependent estimator, our first task is to compute the three-point function of the signal $\tilde{s}_O(t)$ in frequency space, defined as

$$\begin{aligned}\tilde{s}_O\left(f\right) &\equiv \int dt\, e^{-2\pi i f t}\, s_O\left(t\right) \\ &= L \int d^3k\, \mathrm{e}^{-2\pi i \vec{k}\cdot\vec{x}_1} \sum_{\lambda} \mathcal{G}_{\lambda}\left(\hat{k}, \hat{l}_{12}\right) \int dt\, e^{-2\pi i f t}\, h_{\lambda}\left(t - L,\, \vec{k}\right)\, \mathcal{T}\left(kL,\, \hat{k}\cdot\hat{l}_{12}\right) + \tilde{n}_O\left(f\right) \, ,\end{aligned} \tag{46}$$

where $\tilde{n}_O\left(f\right)$ denotes the corresponding noise in frequency space. Defining

$$\tilde{\sigma}_O(f) = \tilde{s}_O\left(f\right) - \tilde{n}_O\left(f\right) \, , \tag{47}$$

we obtain the following three-point function

$$\begin{aligned}\left\langle \tilde{\sigma}_{O_1}(f_1)\, \tilde{\sigma}_{O_2}(f_2)\, \tilde{\sigma}_{O_3}(f_3)\right\rangle = \int \left(\prod_{i=1}^{3} dt_i\, e^{-2\pi i\, f_i t_i}\, d^3k_i \sum c_{ab}^{O_i}\, \mathcal{I}_{ab}^{\lambda_i}(\vec{k}_i)\right) \\ \times \left\langle h_{\lambda_1}(t_1 - L,\, \vec{k}_1)\, h_{\lambda_2}(t_2 - L,\, \vec{k}_2) h_{\lambda_3}(t_3 - L,\, \vec{k}_3)\right\rangle \, ,\end{aligned} \tag{48}$$

whose calculation requires the knowledge of the time correlator for the gravitational waves at unequal times. The expression for the latter quantity is given in Appendix B.

Using eq. (B6) we obtain

$$\begin{aligned}&\int dt_1\, dt_2\, dt_3\, e^{-2\pi i(f_1 t_1 + f_2 t_2 + f_3 t_3)} \left\langle h_{\lambda_1}\left(t_1 - L,\, \vec{k}_1\right) h_{\lambda_2}\left(t_2 - L,\, \vec{k}_2\right) h_{\lambda_3}\left(t_3 - L,\, \vec{k}_3\right)\right\rangle \\ &= \frac{\delta(f_1 + f_2 + f_3)}{32\pi^2}\, \delta^{(3)}\left(\vec{k}_1 + \vec{k}_2 + \vec{k}_3\right) \\ &\times \left\{ f_{\mathrm{NL}}^{\lambda_1,\lambda_2,\lambda_3}\, K_{\lambda_1;\lambda_2,\lambda_3}\left(k_1; k_2, k_3\right) \frac{P_{\lambda_2}\left(k_2\right)}{k_2^3}\, \frac{P_{\lambda_3}\left(k_3\right)}{k_3^3}\, \delta(k_2 - |f_2|)\, \delta(k_3 - |f_3|)\right.\end{aligned}$$

[4] In terms of the parametrization of eqs. (35) and (36) the mirror transformation corresponds to $\{\theta_1,\, \phi_1,\, \phi_2\} \to \{\theta_1,\, -\phi_1,\, -\phi_2\}$.

$$
\begin{aligned}
&+ f_{\rm NL}^{\lambda_2,\lambda_1,\lambda_3}\, K_{\lambda_2;\lambda_1,\lambda_3}\left(k_2; k_1, k_3\right) \frac{P_{\lambda_1}\left(k_1\right)}{k_1^3} \frac{P_{\lambda_3}\left(k_3\right)}{k_3^3}\, \delta(k_1 - |f_1|)\, \delta(k_3 - |f_3|) \\
&+ f_{\rm NL}^{\lambda_3,\lambda_1,\lambda_2}\, K_{\lambda_3;\lambda_1,\lambda_2}\left(k_3; k_1, k_2\right) \frac{P_{\lambda_1}\left(k_1\right)}{k_1^3} \frac{P_{\lambda_2}\left(k_2\right)}{k_2^3}\, \delta(k_1 - |f_1|)\, \delta(k_2 - |f_2|) \Bigg\} \\
&\equiv \delta(f_1 + f_2 + f_3)\, \delta^{(3)}\left(\vec{k}_1 + \vec{k}_2 + \vec{k}_3\right)\, \tilde{\mathcal{B}}_{\lambda_1\lambda_2\lambda_3}(k_1,\, k_2,\, k_3;\, f_1,\, f_2,\, f_3)\,, \qquad (49)
\end{aligned}
$$

so that

$$
\begin{aligned}
\langle \tilde{\sigma}_{O_1}(f_1)\, \tilde{\sigma}_{O_2}(f_2)\, \tilde{\sigma}_{O_3}(f_3)\rangle &= \delta(f_1 + f_2 + f_3) \int \left(\prod_{i=1}^{3} d^3k_i \sum c_{ab}^{O_i}\, \mathcal{I}_{ab}^{\lambda_i}(\vec{k}_i)\right) \\
&\quad \times \delta^{(3)}\left(\vec{k}_1 + \vec{k}_2 + \vec{k}_3\right)\, \tilde{\mathcal{B}}_{\lambda_1\lambda_2\lambda_3}(k_1,\, k_2,\, k_3;\, f_1,\, f_2,\, f_3) \\
&= \delta(f_1 + f_2 + f_3)\, L^3 \int k_1\, dk_1\, k_2\, dk_2\, k_3\, dk_3\, \tilde{\mathcal{B}}_{\lambda_1\lambda_2\lambda_3}(k_1,\, k_2,\, k_3;\, f_1,\, f_2,\, f_3)\, \mathcal{R}_{\lambda_1\lambda_2\lambda_3}^{O_1O_2O_3}(k_1,\, k_2,\, k_3)\,, \qquad (50)
\end{aligned}
$$

where $\mathcal{R}_{\lambda_1\lambda_2\lambda_3}^{O_1O_2O_3}(k_1,\, k_2,\, k_3)$ is the signal three-point response function computed in Section 3.

4.2 The estimator and the optimal SNR

Following [7] we define a frequency-dependent estimator for the three-point function as

$$
\hat{\mathcal{F}}(f_1,\, f_2,\, f_3) \equiv \sum_{ijk} W^{ijk}(f_1,\, f_2,\, f_3)\, \tilde{s}_i(f_1)\, \tilde{s}_j(f_2)\, \tilde{s}_k(f_3)\,, \qquad (51)
$$

where the filter function $W^{ijk}(f_1,\, f_2,\, f_3)$ is totally symmetric, $W^{ijk}(f_1,\, f_2,\, f_3) = W^{jik}(f_2,\, f_1,\, f_3) =$ ..., and satisfies the reality condition $W^{ijk}(f_1,\, f_2,\, f_3)^* = W^{ijk}(-f_1,\, -f_2,\, -f_3)$. Since only the signals $O = \{A,\, E\}$ are relevant for our analysis, only 4 filter functions are independent: W^{AAA}, W^{AAE}, W^{AEE} and W^{EEE}. The frequency integrated estimator $\hat{\mathcal{F}}$ reads

$$
\hat{\mathcal{F}} \equiv \sum_{ijk} \int df_1\, df_2\, df_3 W^{ijk}(f_1,\, f_2,\, f_3)\, \tilde{s}_i(f_1)\, \tilde{s}_j(f_2)\, \tilde{s}_k(f_3)\,, \qquad (52)
$$

with expectation value

$$
\langle \hat{\mathcal{F}} \rangle = \sum_{ijk} \int df_1\, df_2\, df_3 W^{ijk}(f_1,\, f_2,\, f_3)\, \langle \tilde{s}_i(f_1)\, \tilde{s}_j(f_2)\, \tilde{s}_k(f_3)\rangle\,. \qquad (53)
$$

Under the assumptions that the noise is Gaussian[5] (so that its three-point function vanishes) and uncorrelated with the signal, one has $\langle \tilde{s}_i(f_1)\, \tilde{s}_j(f_2)\, \tilde{s}_k(f_3)\rangle = \langle \tilde{\sigma}_i(f_1)\, \tilde{\sigma}_j(f_2)\, \tilde{\sigma}_k(f_3)\rangle$, where $\tilde{\sigma}_i(f)$ is defined in eq. (47). This implies that the expectation value of the estimator is

$$
\begin{aligned}
\langle \hat{\mathcal{F}} \rangle &= \sum_{ijk} \int df_1\, df_2\, df_3 W^{ijk}(f_1,\, f_2,\, f_3)\, \langle \tilde{\sigma}_i(f_1)\, \tilde{\sigma}_j(f_2)\, \tilde{\sigma}_k(f_3)\rangle \\
&= \sum_{ijk} \int df_1\, df_2\, df_3 W^{ijk}(f_1,\, f_2,\, f_3)\, \delta(f_1 + f_2 + f_3)\, S_s^{ijk}(f_1,\, f_2,\, f_3)\,, \qquad (54)
\end{aligned}
$$

[5]This turned out to be the case, for a broad range of frequencies around 1 mHz, in LISA Pathfinder, and is being considered as a working assumption in the LISA Data Challenge (Carlos Fernández Sopuerta, private communication).

where we have defined the real quantity

$$S_s^{ijk}(f_1,\, f_2,\, f_3) \equiv L^3 \sum_{\lambda_1\lambda_2\lambda_3} \int k_1\, dk_1\, k_2\, dk_2\, k_3\, dk_3\, \tilde{\mathcal{B}}_{\lambda_1\lambda_2\lambda_3}(k_1,\, k_2,\, k_3;\, f_1,\, f_2,\, f_3)\, \mathcal{R}^{ijk}_{\lambda_1\lambda_2\lambda_3}(k_1,\, k_2,\, k_3)\,. \tag{55}$$

We next compute the variance of $\hat{\mathcal{F}}$ assuming that the signal is noise dominated, with

$$\langle n_i\,(f_1)\; n_j\,(f_2)\rangle = \delta_{ij}\, P_n^i\,(|f_1|)\; \delta\,(f_1+f_2)\;, \qquad \text{(no sum on } i)\;, \tag{56}$$

(for brevity, from now on we omit the absolute value in the frequency dependence of the noise) so that

$$\begin{aligned}\langle \hat{\mathcal{F}}^2\rangle =& \sum_{ijk} \int df_1\, df_2\, df_3\, \left[6\, W^{ijk}(f_1,\, f_2,\, f_3)\, W^{ijk}(f_1,\, f_2,\, f_3)^* + 9\, W^{ijj}(f_1,\, f_2,\, -f_2)\, W^{ikk}(f_1,\, f_3,\, -f_3)^*\right] \\ & \times P_n^i(f_1)\, P_n^j(f_2)\, P_n^k(f_3)\,,\end{aligned} \tag{57}$$

where the factors of 6 and 9 originate from the symmetry properties of W^{ijk}. The signal-to-noise ratio (SNR) is given by $\langle\hat{\mathcal{F}}\rangle/\sqrt{\langle\hat{\mathcal{F}}^2\rangle}$.

We note that for any given pair of objects $A^{ijk}(f_1,\, f_2,\, f_3)$ and $B^{ijk}(f_1,\, f_2,\, f_3)$ with the properties of our filter function W^{ijk} we can define a scalar product

$$\begin{aligned}\left(A^{ijk},\, B^{ijk}\right) =& \sum_{ijk} \int df_1\, df_2\, df_3\, \left[6\, A^{ijk}(f_1,\, f_2,\, f_3)\, B^{ijk}(f_1,\, f_2,\, f_3)^* + 9\, A^{ijj}(f_1,\, f_2,\, -f_2)\, B^{ikk}(f_1,\, f_3,\, -f_3)^*\right] \\ & \times P_n^i(f_1)\, P_n^j(f_2)\, P_n^k(f_3)\,,\end{aligned} \tag{58}$$

so that we can write the SNR as

$$\mathrm{SNR} = \frac{1}{6}\, \frac{\left(W^{ijk},\, \delta(f_1+f_2+f_3)\, \frac{S_s^{ijk}(f_1,f_2,f_3)}{P_n^i(f_1)\, P_n^j(f_2)\, P_n^k(f_3)}\right)}{\sqrt{(W^{ijk},\, W^{ijk})}}\,. \tag{59}$$

In writing this formula we make the hypothesis that $W^{ijk}(0,\, f_2,\, f_3) = 0$, whose validity will be checked in short, which implies that $\sum_{ijk}\int df_1\, df_2\, df_3 W^{ijj}(f_1,\, f_2,\, -f_2)\, \delta(f_1+f_2-f_2)\, S_s^{ikk}(f_1,\, f_2,\, -f_2) = 0$, i.e., the second term in the scalar product (58) does not contribute to the numerator in eq. (59). The SNR is thus maximized for

$$W^{ijk}(f_1,\, f_2,\, f_3) \propto \delta(f_1+f_2+f_3)\, \frac{S_s^{ijk}(f_1,\, f_2,\, f_3)}{P_n^i(f_1)\, P_n^j(f_2)\, P_n^k(f_3)}\,, \tag{60}$$

up to a multiplicative constant that cancels out from the expression of SNR. This last equation shows that our hypothesis $W^{ijk}(0,\, f_2,\, f_3) = 0$ is valid, since the noise diverges at low frequencies.

The conclusion of this section is that, for this optimal estimator, the SNR is given by

$$\mathrm{SNR} = \left[\frac{T}{6} \sum_{ijk} \int df_1\, df_2\, df_3\, \delta(f_1+f_2+f_3) \sum_{ijk} \frac{S_s^{ijk}(f_1,\, f_2,\, f_3)^2}{P_n^i(f_1)\, P_n^j(f_2)\, P_n^k(f_3)}\right]^{1/2}\,, \tag{61}$$

where T is the duration of the experiment, the indices i, j and k can take only the values A and E and the sum will contain 8 terms.

This relation simplifies in the case in which the channels involved in the correlation have the same noise. The noises of the measurement (22) at the vertex X and at the two other vertices Y and Z of the instrument satisfy

$$\langle n_i(f_1)\, n_j(f_2)\rangle = P_n^{ij}(f_1)\,\delta(f_1+f_2) \quad , \quad \{i,j\}=\{X,Y,Z\} \ . \tag{62}$$

where, due to symmetry[6],

$$\begin{aligned} P_n^{XX}(f) &= P_n^{YY}(f) = P_n^{ZZ}(f) \equiv P_{n,\text{self}}(f) \ , \\ P_n^{XY}(f) &= P_n^{XZ}(f) = P_n^{YZ}(f) \equiv P_{n,\text{cross}}(f) \ . \end{aligned} \tag{63}$$

The linear combinations (25) have diagonal noise (56), with spectral dependence

$$\begin{aligned} P_n^A(f) &= P_n^E(f) = \frac{2}{3}\left[P_{\text{n,self}}(f) - P_{\text{n,cross}}(f)\right] \equiv (2L)^2 P_n(f) \ , \\ P_n^T(f) &= \frac{1}{3}\left[P_{\text{n,self}}(f) + 2\,P_{\text{n,cross}}(f)\right] \ , \end{aligned} \tag{64}$$

which shows that the A and E channels have indeed identical noise. The factor $(2L)^2$ has been inserted in the definition of $P_n(f)$ so to convert from time displacement to strain, by dividing ΔT by the round-trip light travel distance $2L$ [20]. In this way, $P_n(f)$ has the dimension of time.

Using these two channels, the relation (61) can be explicitly written as

$$\begin{aligned} \text{SNR} = \Bigg\{ \frac{T}{6}\sum_{ijk}\int \frac{df_1\,df_2\,df_3}{(4L^2)^3\,P_n(f_1)\,P_n(f_2)\,P_n(f_3)}\,\delta(f_1+f_2+f_3) \Bigg[S_s^{AAA}(f_1,\,f_2,\,f_3)^2 \\ +3\,S_s^{AAE}(f_1,\,f_2,\,f_3)^2 + 3\,S_s^{AEE}(f_1,\,f_2,\,f_3)^2 + S_s^{EEE}(f_1,\,f_2,\,f_3)^2 \Bigg] \Bigg\}^{1/2} \ , \end{aligned} \tag{65}$$

where the factors of 3 in front of S_s^{AAE} and S_s^{AEE} originate from equalities such as $S_s^{AAE} = S_s^{AEA} = S_s^{EAA}$.

4.3 SNR for a non-Gaussian signal enhanced at a fixed scale

As an explicit example of application of these results, in this subsection we evaluate the SNR (65) for a specific shape of non-Gaussian bispectrum. We make the following choice of kernel entering in eq. (6):

$$K_{\lambda_1;\lambda_2,\lambda_3}(k_1;k_2,k_3) = \mathrm{e}^{-\frac{1}{2\sigma^2}\left[(k_1-k_*)^2+(k_2-k_*)^2+(k_3-k_*)^2\right]}\delta_{\lambda_1 L}\,\delta_{\lambda_2 L}\,\delta_{\lambda_3 L} \ . \tag{66}$$

where we assume that $\sigma \ll k_*$, and normalize the shape function to one at its maximum. This localized, chiral bump in non-Gaussianity well approximates the predictions of certain models of Early Universe cosmology, for instance the signal obtained in the model of [21] that we will review in the subsection 5.2.

We can use this kernel in the expressions for the SNR we developed in Section 4. We relegate technical steps of the calculations to Appendix D, and write here the final expression for the SNR:

[6]The cross-correlation arises because the different interferometers share one common arm.

$$\text{SNR} \simeq \frac{f_{\rm NL}^{LLL}}{256\,\pi^2}\,\frac{\sqrt{2}\pi\,\sigma^2}{k_*^3}\,P_L^2\,(k_*)\,\sqrt{\frac{T}{P_n^2\,(k_*)\;P_n\,(2k_*)}} \times\sqrt{\mathcal{R}_{LLL}^{AAA}\,(k_*,\,k_*,\,k_*)^2+3\mathcal{R}_{LLL}^{AAE}\,(k_*,\,k_*,\,k_*)^2+3\mathcal{R}_{LLL}^{AEE}\,(k_*,\,k_*,\,k_*)^2+\mathcal{R}_{LLL}^{EEE}\,(k_*,\,k_*,\,k_*)^2}\;. \tag{67}$$

The equilateral transfer functions are plotted in the left panel of Fig. 3. We assume that k_* is sufficiently small, so that we can use the low-frequency asymptotically constant values that can be observed from the figure. This is the case for, approximately, $k_* L \lesssim 0.05$, or, taking $L = 2.5 \times 10^6\,\text{km} \simeq \frac{1}{0.12\,\text{Hz}}$, for $k_* \lesssim 0.006\,\text{Hz}$. In the following we assume that k_* satisfies this inequality. Then, $\left\{\left(\mathcal{R}_{LLL}^{AAA}\right)^2+3\left(\mathcal{R}_{LLL}^{AAE}\right)^2+3\left(\mathcal{R}_{LLL}^{AEE}\right)^2+\left(\mathcal{R}_{LLL}^{EEE}\right)^2\right\}^{1/2} \simeq 4.3$, and we can write

$$\begin{aligned}\text{SNR} &\simeq 0.0076\,f_{\rm NL}^{LLL}\,\frac{\sigma^2}{k_*^3}\,P_L^2\,(k_*)\,\left\{\frac{T}{P_n\,(k_*)\,P_n\,(k_*)\,P_n\,(2k_*)}\right\}^{1/2} \\ &\simeq 7.9\times10^5\,f_{\rm NL}^{LLL}\,\frac{\sigma^2}{k_*^2}\,\left(\frac{10^{-3}\,\text{Hz}}{k_*}\right)^5\left(\Omega_{\rm GW}\,(k_*)\,h^2\right)^2\,\frac{10^{-40}\,\text{Hz}^{-1}}{P_n\,(k_*)}\,\sqrt{\frac{T}{3\,\text{yrs}}\,\frac{10^{-40}\,\text{Hz}^{-1}}{P_n\,(2k_*)}}\;.\end{aligned} \tag{68}$$

where in the second line we normalize the various quantities to useful reference values, to be able to more easily appreciate the relevance of the result. For definiteness, we normalize k_* to $10^{-3}\,\text{Hz}$, where (parametrically) the sensitivity of LISA is greatest; we then normalize the noise function to $10^{-40}\,\text{Hz}^{-1}$, which is (parametrically) the value obtained in this frequency range (see for instance Fig. 3 of [20], where the square root of P_n is shown; we note that the noise power spectrum P_n is related to the sensitivity S_n by $P_n = \mathcal{R}_2\,S_n$, where $\mathcal{R}_2$ is the two-point response function shown in Fig. 2.). We normalize the time to the nominal LISA mission time of 4 years times a 75% duty factor.

In the above relation, we also traded the GW power spectrum for the fractional GW contribution to the energy density of the universe per logarithmic wavenumber interval. Using the expression $\rho_{\rm GW} = \frac{M_p^2}{4}\left\langle \dot{h}_{ij}\dot{h}_{ij}\right\rangle$ for the energy density in GW, one finds

$$\Omega_{\rm GW}\,(k) \equiv \frac{1}{3H_0^2M_p^2}\,\frac{\partial\rho_{\rm GW}}{\partial\ln k} = \frac{\pi^2}{3}\,\frac{k^2}{H_0^2}\,\sum_\lambda P_\lambda\,(k)\;. \tag{69}$$

where $H_0 \simeq 3.24\times10^{-18}\,h\,\text{Hz}$ is the present value of the Hubble rate. This expression was used to obtain the second line of (68).

As discussed in Section 2, the value of the non-linear parameter entering in this relation is the present one, related to the primordial one by eq. (10). A detailed discussion of the transfer functions entering in this relation can be found for instance in [22]. The precise behavior is not needed for the present estimate. When they are well outside the horizon, the GW have constant amplitude; instead the amplitude decreases as the inverse power of the scale factor while it is well inside the horizon. For the present estimate can simply take $\mathbf{T}\,(t_0,\,k) = a_k$, leading to

$$\text{SNR} \simeq 7.9\times10^5\,\frac{f_{\rm NL}^{LLL,\text{primordial}}}{a_{k_*}}\,\frac{\sigma^2}{k_*^2}\,\left(\frac{10^{-3}\,\text{Hz}}{k_*}\right)^5\left(\Omega_{\rm GW}\,(k_*)\,h^2\right)^2\,\frac{10^{-40}\,\text{Hz}^{-1}}{P_n\,(k_*)}\,\sqrt{\frac{T}{3\,\text{yrs}}\,\frac{10^{-40}\,\text{Hz}^{-1}}{P_n\,(2k_*)}}\;. \tag{70}$$

We recall that, in the case of GWs produced during inflation, a_{k_*} is the value of the scale factor when the mode of frequency k_* re-entered the horizon in the Friedmann-Lemaître-Robertson-Walker (FLRW) stage after inflation (we normalize the scale factor to one today). The same relation applies for GW modes that are produced when their size is comparable to the horizon side during radiation domination. Assuming that the universe is radiation dominated at that moment, and that radiation domination continues until the recent stage matter-radiation equality (at $z_{\rm eq} \sim 3,400$) we find (see Appendix E)

$$\left.{\rm SNR}\right|_{\rm from\ inflation} \simeq 1.6 \times 10^{-3}\, f_{\rm NL}^{LLL,{\rm primordial}}\, \frac{\sigma^2}{k_*^2} \left(\frac{10^{-3}\,{\rm Hz}}{k_*}\right)^4 \left(\frac{\Omega_{\rm GW}\left(k_*\right) h^2}{10^{-13}}\right)^2 \times \frac{10^{-40}\,{\rm Hz}^{-1}}{P_n\left(k_*\right)} \sqrt{\frac{T}{3\,{\rm yrs}}\, \frac{10^{-40}\,{\rm Hz}^{-1}}{P_n\left(2k_*\right)}}\,. \tag{71}$$

As we discuss in Appendix E, modes that have presently the frequency $k = 10^{-3}\,{\rm Hz}$ re-entered the horizon at the temperature of $\sim 50\,{\rm TeV}$. A different value for a_* can be obtained if we make instead the unconventional hypothesis that the universe had a different equation of state than radiation, before, but close, to Big-Bang Nucleosynthesis.

A different value for a_* is instead obtained if we assume that GW are produced inside the horizon by a sudden episode that took place during radiation domination at the temperature T_*. In this case we find (see Appendix E)

$$\left.{\rm SNR}\right|_{\rm production\ inside\ horizon} \simeq 3 \times 10^{-6}\, f_{\rm NL}^{LLL,{\rm primordial}}\, \frac{T_*}{100\,{\rm GeV}}\, \frac{\sigma^2}{k_*^2} \left(\frac{10^{-3}\,{\rm Hz}}{k_*}\right)^5 \left(\frac{\Omega_{\rm GW}\left(k_*\right) h^2}{10^{-13}}\right)^2 \times \frac{10^{-40}\,{\rm Hz}^{-1}}{P_n\left(k_*\right)} \sqrt{\frac{T}{3\,{\rm yrs}}\, \frac{10^{-40}\,{\rm Hz}^{-1}}{P_n\left(2k_*\right)}}\,. \tag{72}$$

The previous result is recovered if we take $T_* = 50\,{\rm TeV}$.

In both these relations, $\Omega_{\rm GW}\left(k_*\right) h^2$ has been normalized to the threshold level that can be detected in the 2-point correlation function at LISA. Finally, we recall that these results assume $k_* \lesssim 0.006\,{\rm Hz}$, as we have taken the low-frequency asymptotic value for the transfer functions. However, they can be immediately generalized for higher frequencies, by using the appropriate value for the combination $\left\{\left(\mathcal{R}_{LLL}^{AAA}\right)^2 + 3\left(\mathcal{R}_{LLL}^{AAE}\right)^2 + 3\left(\mathcal{R}_{LLL}^{AEE}\right)^2 + \left(\mathcal{R}_{LLL}^{EEE}\right)^2\right\}^{1/2}$.

5 Tensor non-Gaussianity and Early Universe Cosmology

In the previous sections, we developed techniques for investigating the non-Gaussianity of a SGWB by studying the three-point correlation function of signals detectable with LISA. We have shown that LISA is in principle able to measure specific properties of the SGWB bispectra, as the dependence on the amplitude of the momentum and polarization of the GW signal.

In this section we review and discuss the current theoretical understanding of non-Gaussian features of a primordial SGWB sourced by Early Universe physics, in particular inflation and cosmological defects. Our aim is to provide theoretical motivations for the results derived in the previous Sections,

showing that they can be used to distinguish different sources for primordial SGWBs. Besides analyzing models, we also briefly review current and perspective constraints on tensor non-Gaussianity from the physics of CMB, that is able to probe primordial SGWBs at frequency scales much smaller than interferometers.

5.1 Primordial tensor non-Gaussianity and inflationary physics

Cosmological inflation predicts the existence of a stochastic background of tensor modes, produced by quantum fluctuations of the metric spin-2 degrees freedom during the phase of inflationary expansion. CMB experiments constrain the amplitude of the primordial SGWB power spectrum at large CMB scales in terms of the tensor-to-scalar ratio r: the current upper bound from BICEP2/Keck and Planck is $r < 0.07$ at 95% confidence level [23, 24] (assuming the consistency relation $r = -8n_T$), and future CMB polarization experiments [25–27] can lower this bound down to around 10^{-3} in absence of a detection.

Tensor self-interactions are expected to make the non-Gaussianity of the primordial SGWB relatively large, already within Einstein gravity. Moreover, as we shall review next, there are models of inflation which exploit specific couplings between fields present during the inflationary era, in order to enhance the amplitude of the tensor power spectrum at scales that can be probed by the future generation of gravitational interferometers. This gives the opportunity to probe inflation at scales much smaller than CMB scales: in these scenarios, the large couplings among the fields involved can enhance tensor non-Gaussianity, making it a very useful observable for distinguishing among different scenarios. We briefly survey the topic of inflationary tensor non-Gaussianity, considering in succession models of increasing complexity.

General Relativity in pure de Sitter space

The simplest situation to investigate – as a toy model for inflation – is pure General Relativity (GR) in de Sitter space. The metric for de Sitter space can be expressed as $ds^2 = -dt^2 + e^{2Ht}d\vec{x}^2$, with H the constant Hubble parameter. As we have seen in Section 2, the transverse-traceless spin-2 tensor fluctuations can be decomposed in two helicity modes, $\lambda = L$ (left) and $\lambda = R$ (right). The Einstein-Hilbert action

$$S_{EH} = \int d\tau\, d^3x\, \sqrt{-g}\, \left[\frac{M_{Pl}^2}{2} R - \Lambda\right] , \tag{73}$$

can be straightforwardly expanded around the de Sitter background up to third order in fluctuations [12,28]. From the second order action one can compute the two-point function for the Fourier transform of the tensor fluctuations, which defines the primordial tensor power spectrum

$$\left\langle h_\lambda\left(t, \vec{k}\right) h_{\lambda'}\left(t, \vec{k}'\right)\right\rangle = \frac{P_\lambda(k)}{4\pi k^3}\, \delta_{\lambda\lambda'}\, \delta^{(3)}\left(\vec{k} + \vec{k}'\right) , \tag{74}$$

$$P_\lambda(k) = \frac{1}{\pi^2}\left(\frac{H}{M_{Pl}}\right)^2 . \tag{75}$$

From the third order action one obtains the three-point function for the fluctuations [12, 28], which defines the primordial tensor bispectrum

$$\left\langle \hat{h}_{\lambda_1}\left(t, \vec{k}_1\right) \hat{h}_{\lambda_2}\left(t, \vec{k}_2\right) \hat{h}_{\lambda_3}\left(t, \vec{k}_3\right)\right\rangle = \delta^{(3)}\left(\vec{k} + \vec{k}_2 + \vec{k}_3\right) \mathcal{B}_{\lambda_1,\lambda_2,\lambda_3}\left(k_1, k_2, k_3\right) , \tag{76}$$

and can be obtained using for example the in-in formalism. The tensor bispectrum is the lowest order statistics providing information on non-Gaussianity of tensor fluctuations. Its dependence on the three wave-vectors characterizes the shape of tensor non-Gaussianity, one of the properties that allows one to distinguish among different models. We list here some properties of the tensor bispectrum and the corresponding tensor non-Gaussianities for GR in de Sitter space:

1. The amplitude of tensor non-Gaussianity – parameterized by the ratio between the tensor bispectrum and the square of the tensor power spectrum – are of order one in pure GR (but not larger). For example, one finds [29]

$$\frac{B_{RRR}(k,\,k,\,k)}{P_R^2(k)} \simeq 3.6\,. \tag{77}$$

   This is a difference with respect to scalar curvature fluctuations in single field vanilla models of inflation, where scalar non-Gaussianities are suppressed by slow-roll parameters, and are then at most of order a few percent [8, 9, 12, 13]. This is due to the fact that Einstein gravity is a non-linear theory, and cubic interactions are not suppressed with respect to quadratic ones by small (e.g. slow-roll) parameters. In Einstein gravity the shape of tensor bispectra is peaked in squeezed configurations.

2. The amplitude of tensor bispectra depends on chirality, that is on the polarization indexes L, R, and in general bispectra characterized by different indexes have different amplitudes. For example, in the case of GR in de Sitter space one finds [29, 30]

$$B_{RRL}(k,k,k) \,=\, \frac{B_{RRR}(k,k,k)}{81}\,. \tag{78}$$

   This is different with respect to the power spectrum, where L and R modes have the same amplitude (see eq. (75)) and the cross correlation vanishes, $\langle h_L\, h_R\rangle = 0$. This has interesting phenomenological consequences since we have many independent bispectrum components we can use to build observables for distinguishing among different models of inflation. As we have learned in Section 3, LISA can in principle probe different chiral components of primordial bispectra.

3. Pure Einstein gravity around de Sitter space *preserves parity*, in the sense that the amplitudes of power spectrum and bispectrum components obtained interchanging all the L, R indexes is the same. For example, $P_L(\vec{k}) = P_R(-\vec{k})$, $B_{LLL}(\vec{k}_i) = B_{RRR}(-\vec{k}_i)$, $B_{LLR}(\vec{k}_i) = B_{RRL}(-\vec{k}_i)$ etc. This is potentially not true in more complex inflationary scenarios, as we are going to discuss in the following subsection.

We can go beyond a pure Einstein-Hilbert action, and investigate non-Gaussian tensor fluctuations around de Sitter space in theories of gravity including higher order curvature invariants [28, 31, 32], schematically denoted as $\int W^3$ and $\int \tilde{W} W^2$ ($W_{\mu\nu\rho\sigma}$ being the Weyl tensor). Such perturbative contributions modify the third-order tensor action, and lead to new, parity preserving shapes for the tensor bispectra. However, their amplitudes can not be (much) larger than the ones one finds within General Relativity, due to unitarity constraints.

Single field slow-roll inflation

An enhanced amplitude of tensor bispectra can be obtained in single field inflation, with the time variable controlled by a scalar field, the inflaton. The power spectrum of tensor modes in single-field slow-roll models of inflation is straightforward to compute, and one finds the same result as in de Sitter space, but with an additional scale dependence. In the simplest models of inflation the tensor spectrum is red, with a spectral tilt given by

$$n_T \,=\, -r/8\,, \tag{79}$$

with r the tensor-to-scalar ratio [7]. The analysis of the tensor bispectrum is instead less straightforward: the scalar can have non-minimal derivative couplings with the metric – see e.g. the model [34] built in terms of the Horndeski theory – which can complicate the analysis. The complete classification of tensor non-Gaussianity in single field models of inflation based on Horndeski scalar-tensor theories of gravity has been done in [30], finding that besides the Einstein-Hilbert part [12], the third order action for tensor modes acquires a parity-preserving contribution proportional to the cube of time derivatives of tensor fluctuations:

$$S^{new}_{(3)} \,=\, \int dt\, d^3x\, G(a,\,\phi)\, \dot{h}_{ik}\dot{h}_{kl}\dot{h}_{li}\,, \tag{80}$$

where G is a function of the scale factor and of the homogeneous profile of the scalar field and its first time derivatives (it is related with the function G_5 controlling the quintic Horndeski action). Interestingly, there are no obvious unitarity constraints on the size of this correction to the Einstein-Hilbert action, hence – depending on the inflationary model and the profile for the scalar field – this contribution can lead to a tensor bispectrum whose amplitude is parametrically larger than the GR result (although it might be hard to find an explicit model satisfying all the CMB constraints in the scalar sector). The shape of the tensor bispectrum has been investigated in [30], finding that it is maximized for equilateral configurations, hence it is different from the GR one, maximized in the squeezed limit. In the equilateral limit, the bispectrum components associated with action (80) satisfy the relation

$$B^{(new)}_{RRL}(k,k,k) \,=\, \frac{B^{(new)}_{RRR}(k,k,k)}{9}. \tag{81}$$

This is different from the GR result of eq (78): we learn that the chiral structure of the tensor bispectra – i.e. a distinctive hierarchy for the amplitudes of the tensor bispectra depending on the polarization indexes L, R – might be used to build observables to distinguish among different models.

Tensor non-Gaussianity in single field models of inflation based on generalization of Horndeski actions [35–40] is a topic still under investigation, see e.g. [41], and also [42] for an analysis carried on using techniques based on effective field theory for inflation. Also, tensor non-Gaussianity in parity-violating scalar-tensor theories [43,44] that spontaneously break Lorentz invariance [45] is particularly interesting to motivate a search of parity violating effects in the tensor bispectrum: an analysis of the tensor bispectrum in parity violating gravitational theories can be found in [31,32,46], although their generalization to the extended set-up introduced in [45] is still an open question.

Beyond single field inflation

Since the simplest single field models of inflation predict a red tensor tilt, the amplitude of the primordial SGWB is too small to be detected with interferometers. On the other hand, there are more

[7] Equation (79) holds at leading order in slow-roll for inflationary models with unit tensor sound speed. See [33] for a systematic discussion of more general scenarios that can change this relation.

complex inflationary scenarios that might allow one to enhance the tensor spectrum at interferometer scales [33, 47], and that may lead to large tensor non-Gaussianity with distinctive features. We briefly discuss here two frameworks, whose predictions for the tensor bispectrum have been studied so far:

Coupling the inflaton with additional scalars and vector fields

If other sources of GWs are present during inflation, the primordial SGWB can have richer features. A possibility to source primordial GWs is to couple fields driving inflation with additional scalars [48–53], $U(1)$ gauge vectors [54–57], non-Abelian vector fields [58–68], or Standard Model fields [69]. These mechanisms usually exploit instabilities for the additional source fields during inflation. Such instabilities feed in the evolution of tensor modes through higher order contributions to the anisotropic stress, and affect both power spectra and bispectra of fluctuations: see e.g. [21, 70–72]. Given the nature of the couplings, the resulting tensor power spectrum and bispectra can be parity violating, and the bispectra are usually enhanced in equilateral configurations. The tensor power spectrum profile can acquire a feature (a 'bump' profile) and can also get sufficiently enhanced at small scales to be detected with interferometers [47]. Models involving couplings between (pseudo)scalars and gauge fields are theoretically well understood, and their observational prospects in CMB polarization and interferometer experiments are being developed in great detail, in particular for what respect the parity violating features of power spectra and bispectra, see e.g. the recent papers [65, 73] and references therein.

Breaking space-time symmetries during inflation

Another possibility for enhancing the bispectrum of tensor modes is to break space-time symmetries during inflation. One way to do so are scenarios of (super)solid inflation: see e.g. [74–83], where the vacuum expectation value of additional scalar fields spontaneously breaks space diffeomorphisms during inflation, or more in general in models where spatial diffeomorphisms are broken spontaneously during inflation. Tensor bispectra are maximized in squeezed configurations, and their amplitude can be parametrically larger than in Einstein gravity. In the scenarios explored so far in the literature, power spectrum and bispectrum components are all parity preserving.

Alternatively, space-time symmetries can be broken *explicitly* as for example a violation of Lorentz symmetry in Hořava-Lifshitz gravity: in this case inflationary tensor fluctuations are automatically chiral [84] and the tensor bispectra can be chiral and enhanced with respect to GR results [85, 86].

For these systems, some additional mechanisms (as growth of perturbations due to instabilities) might be necessary to amplify the tensor spectrum at interferometer scales.

5.2 An explicit example: tensor non-Gaussianity and axion inflation

After the general survey of the previous subsection, we describe in detail the predictions of a concrete model able to produce a signal detectable at interferometers with large tensor non-Gaussianity. We assume that during inflation, which is driven by a scalar ϕ, an auxiliary axion field χ interacts with a gauge field A_μ: the Lagrangian density for the system is

$$\mathcal{L} = -\frac{1}{2}\left(\partial\phi\right)^2 - V\left(\phi\right) - \frac{1}{4}F_{\mu\nu}F^{\mu\nu} - \frac{\chi}{f}F_{\mu\nu}\tilde{F}^{\mu\nu}\,, \tag{82}$$

where $1/f$ is a coupling constant with the dimension of a length, and $F_{\mu\nu}$ ($\tilde{F}^{\mu\nu}$) is the field (dual) strength tensor. GW non-Gaussianities in different helicity channels become larger than those of

the scalar perturbations by different orders of magnitudes. This can be understood easily noticing that both scalar and tensors are sourced with similar efficiency (and source) but the scalars are suppressed by the helicity conservation, while the tensors can be large and also chiral, meaning that the contribution of the different correlator are different for different combinations of the helicity.
In such a model the gauge field A_μ acts as a source for both scalar and tensor metric perturbations, and, for the latter, this translates into a source term in the equation of motion of h_{ij}

$$h_{ij}'' + 2\,\frac{a'}{a}\,h_{ij}' - \Delta\, h_{ij} = \frac{2}{M_P^2}\,\Pi_{ij}{}^{lm}\,T_{lm}^{EM}\,, \tag{83}$$

where $\Pi_{ij}{}^{lm} = \Pi_l^i\,\Pi_m^j - \frac{1}{2}\Pi_{ij}\,\Pi^{lm}$ is the transverse traceless projector, with $\Pi_{ij} = \delta_{ij} - \partial_i\,\partial_j/\Delta$ and where T_{lm}^{EM} represents the spatial part of the stress-energy tensor of the gauge field. The source term arises not from the $F\tilde{F}$ term but from the FF term in eq. (82). Parity-violating information of the gauge field is transmitted through this source term to the tensors that acquire a chiral component. The GW solution for such equation can be found using the Green function method, see [87,88].

Using the same procedure as described in [54, 87] we can compute both the two-point function and the three-point function at super-horizon scales ($k\tau \to 0$) for the tensor modes. The GW two-point function receives contributions from the parity conserving amplification of vacuum fluctuations and from the excited electromagnetic modes which source the parity violating parts. These two contributions are uncorrelated and the overall right- and left-handed power spectra are

$$\begin{aligned} P_R &= \frac{H^2}{\pi^2 M_{Pl}^2}\left(1 + 8.6\times 10^{-7}\,\frac{H^2}{M_{Pl}^2}\,\frac{e^{4\pi\xi}}{\xi^6}\right)\,, \\ P_L &= \frac{H^2}{\pi^2 M_{Pl}^2}\left(1 + 8.6\times 10^{-9}\,\frac{H^2}{M_{Pl}^2}\,\frac{e^{4\pi\xi}}{\xi^6}\right)\,, \end{aligned} \tag{84}$$

where the parameter ξ encodes the velocity of the field χ, $\xi = \dot{\chi}/(2fH)$. For the three-point function, at late times ($k\tau \to 0$), we have

$$\begin{aligned} \langle h_{\lambda_1}(\mathbf{k_1})\,h_{\lambda_2}(\mathbf{k_2})\,h_{\lambda_3}(\mathbf{k_3})\rangle &= 4\,\delta(\mathbf{k_1}+\mathbf{k_2}+\mathbf{k_3})\int d^3\mathbf{q}\,F_{\lambda_1}(\mathbf{k_1},\,\mathbf{q})\,F_{\lambda_2}(\mathbf{k_2},\,-\mathbf{q})\,F_{\lambda_3}(\mathbf{k_3},\,\mathbf{q}-\mathbf{k_1}) \\ &\quad + (\mathbf{k_2}\leftrightarrow\mathbf{k_3})\,, \end{aligned} \tag{85}$$

where the function $F_\lambda^{lm}(\mathbf{k},\,\mathbf{q})$ is the same as in [87]. The largest contribution to the three-point function of the GW, given by the $\langle h_R h_R h_R\rangle$ correlator, was already computed in [87,89], where was also shown that the shape of such a bispectrum peaks in the equilateral limit ($|\mathbf{k_1}| = |\mathbf{k_2}| = |\mathbf{k_3}| = k$). Here we extend such computations to estimate the amplitude of the other mixed contributions to the GW bispectrum, which are

$$\begin{aligned} \langle h_R(\mathbf{k}_1)\,h_R(\mathbf{k}_2)\,h_R(\mathbf{k}_3)\rangle_{\rm equil} &\simeq -5.7\times 10^{-10}\,\frac{H^6}{M_P^6}\,\frac{e^{6\pi\xi}}{\xi^9}\,\frac{\delta(\mathbf{k_1}+\mathbf{k_2}+\mathbf{k_3})}{k^6}\,, \\ \langle h_L(\mathbf{k}_1)\,h_R(\mathbf{k}_2)\,h_R(\mathbf{k}_3)\rangle_{\rm equil} &\simeq -9.0\times 10^{-12}\,\frac{H^6}{M_P^6}\,\frac{e^{6\pi\xi}}{\xi^9}\,\frac{\delta(\mathbf{k_1}+\mathbf{k_2}+\mathbf{k_3})}{k^6}\,, \\ \langle h_L(\mathbf{k}_1)\,h_L(\mathbf{k}_2)\,h_R(\mathbf{k}_3)\rangle_{\rm equil} &\simeq 1.9\times 10^{-15}\,\frac{H^6}{M_P^6}\,\frac{e^{6\pi\xi}}{\xi^9}\,\frac{\delta(\mathbf{k_1}+\mathbf{k_2}+\mathbf{k_3})}{k^6}\,, \\ \langle h_L(\mathbf{k}_1)\,h_L(\mathbf{k}_2)\,h_L(\mathbf{k}_3)\rangle_{\rm equil} &\simeq -1.2\times 10^{-14}\,\frac{H^6}{M_P^6}\,\frac{e^{6\pi\xi}}{\xi^9}\,\frac{\delta(\mathbf{k_1}+\mathbf{k_2}+\mathbf{k_3})}{k^6}\,. \end{aligned} \tag{86}$$

Note that the signs and reality condition are specific to our choice of chiral polarization operators varying the properties in eq. (3).

We find that the mixed helicity components are non-zero and in Section 4 we have seen how LISA is sensitive to such components. The shape of the GW three-point functions is close to equilateral and this can be explained by the fact that the mechanism of generation of perturbations happens at sub-horizon scales.

5.3 Primordial tensor non-Gaussianity at CMB scales

To put our investigation in a wider context, we discuss in this subsection the current and perspective constraints on tensor non-Gaussianity from CMB physics. CMB observations at large scales impose stringent constraints on the non-Gaussianity of scalar curvature (density) perturbations, and have the potential to constrain tensor non-Gaussianity as well, but at frequencies much smaller than interferometer scales. The tightest constraints come from the *Planck* collaboration [6], setting strong limits on scalar non-Gaussianity for a variety of well-motivated models. For example, for the "standard" local, equilateral and orthogonal shapes the analysis of *Planck* temperature (T) and E-mode polarization data constrain the level of these types of non-Gaussianity to $f_{NL}^{local} = 0.8 \pm 5.0$, $f_{NL}^{equil} = -4 \pm 43$ and $f_{NL}^{ortho} = -26 \pm 21$ (68% CL, statistical) from the measurements of the angular CMB bispectrum. These values point into the direction of consistency with the predictions of the standard cosmological model based on single-field models of slow-roll inflation, meaning that the structure that we observe today have been sourced by (almost) Gaussian seed perturbations. However there are also much less studied observables that could open up a new window into the physics of the early universe in the near future. Among these there are non-Gaussian signatures coming from tensor (gravitational waves) 3-point correlations, and also non-Gaussianity coming from mixed (tensor-scalar) 3-point correlators. Interesting bounds on these kind of signals already exist. A first observational limit on the tensor non-linearity parameter f_{NL}^{tens} has been obtained by *Planck* (from temperature data): $f_{NL}^{tensor}/10^2 = 4 \pm 15$ (68%CL), which is consistent with a previous WMAP data analysis [90]. The tensor bispectra analyzed derive from some models of inflation predicting a specific parity violation in the tensor sector. However, future observations of CMB will try to improve constraints on tensor fluctuations focusing on B-mode polarization. The reason is that in this case primordial tensor modes are not hidden by scalar perturbations. The main contamination to the B mode polarization signal is polarized dust [91] and lensing of the E-modes to B-modes [92]. However, precise B-mode measurements have just started and the prospects of improvement are large. For example the constraints on the $\langle BTT \rangle$ CMB bispectrum arising from mixed correlators tensor-scalar-scalar can improve by an order of magnitude with a CMB-Stage IV mission w.r.t the ones achievable from temperatura data alone (see, e.g., [93]). Observational constraints on such a primordial tensor-scalar-scalar bispectrum already exist and have been obtained recently in [94] using WMAP temperature data finding a constraint $g_{tss} = -48 \pm 28$ (68%CL) on the amplitude of such interactions. The inclusion of polarization information will certainly improve such a constraint. On the other hand it might be crucial to have the possibility to probe such signals on different scales, like the ones which are probed by direct measurements from interferometers. This might serve not only as a possible consistency check, but also to test models of inflation that eventually produce a relevant bispectrum signature only at interferometric scales.

5.4 Other early Universe mechanisms sourcing gravitational waves

So far in Section 5, we have considered GW backgrounds from inflation which can lead to a significant deviation from Gaussian statistics. Inflation, however, is not the only source of GWs from the early Universe. Various post-inflationary mechanisms can be also responsible for the generation of GW backgrounds having today a large amplitude. Non-linear field dynamical processes after inflation can generate non-trivial quadrupolar field distributions, resulting in an active and efficient source of GWs. The most representative processes are non-perturbative particle production [95–102], strong first order phase transitions [103–109] and cosmic defect networks [110–116]. For a recent review on early Universe GW sources see [3].

The stochastic background of GWs from strong first order phase transitions is expected to exhibit a single "bump" spectrum, with a rather large amplitude, depending on the efficiency of the dynamical processes involved in the emission of GWs. In particular, if the electroweak phase transition is sufficiently strong due to the presence of beyond the Standard Model (SM) particle physics, the peak frequency of the associated GW background lies naturally within the LISA frequency window. For a discussion on the ability of LISA to measure a GW background from first order phase transitions (and in particular from the electroweak phase transition) see [3, 108]. The stochastic background of GWs from non-perturbative phenomena like periodic [101, 117], tachyonic [99, 100] or other [102, 118, 119] excitation of fields (typically expected in preheating), is also characterized by a single "bump" spectrum, with an amplitude that can be typically large but peaked at very high frequencies (unless extreme fine tuned couplings are considered). In both cases, phase transitions and preheating, the production of GWs is due to a causal process. This implies that today's background is formed by the superposition of billions of independent signals (corresponding to the GWs emitted from the many uncorrelated regions at the time of the background generation), and hence it must have necessarily a Gaussian distribution, due to the central limit theorem. The angular resolution needed to probe any of the individual signals, beyond their effective stochastic Gaussian nature, is far beyond the reach of any reasonable GW detector. GW backgrounds from preheating and phase transitions are therefore expected to be highly Gaussian, and hence their 3-point function is expected to vanish at the data of any interferometer. For a discussion on this aspect, see Section 3.1 of Ref. [3].

The case of GW emission from cosmic defect networks is however very different. The GW signal expected from cosmic defects can be the sum of two components. The first component is the emission of GWs produced around the horizon at each time t, by the anisotropic stress of the network [115, 120–123]. This first component is expected to be emitted by any network of cosmic defects in *scaling*, independently of the topology and origin of the defects [115]. The second contribution is only expected for a network of cosmic strings – local gauge one-dimensional topological defects – and is given by the superposition of GWs emitted from sub-horizon strings chopped off from the string network all along cosmic history, as well as from super-horizon strings with superimposed small-scale structure [111] due to string interconnections leading to kink formation. For a cosmic string network, this second contribution is expected to be the dominant one. However, the argument of causality discussed above, remains valid, even if the GWs are continuously emitted during several Hubble times. Thus, this background cannot be resolved beyond its stochastic nature, and is expected to be Gaussian[8]. We

[8] In reality, on top of the continuous stochastic Gaussian background from cosmic strings, there can be individual bursts emitted by nearby strings or a "popcorn" discontinuous noise. The former results from the fact that at small redshifts there are not many sources and events do not overlap, thus the time interval between events is longer than the duration of a single event. The latter is a noise generated by rare bursts at high redshifts leading to unresolved GW sources. Considering the number of sources at a given frequency as a Poisson process, one may thus expect either to get

therefore expect that any non-Gaussianity in the continuous stochastic background sourced by a defect network, can only be due to the first contribution (even if this is sub-dominant in the case of cosmic strings, in terms of the power spectrum).

Let us thus focus on the first contribution mentioned above, produced by the anisotropic stress of a defect network. This contribution represents an irreducible emission of GWs sourced by any type of viable defect network that reached scaling, meaning that the energy density in the defect network is constant fraction of the overall energy density of the Universe. Such defects can be either one-dimensional topological defects — global, Abelian, non-Abelian, semi-local strings — or (viable) global defects — domain walls, monopoles or non-topological textures [115]. Indeed, in the case of local strings, scaling is reached by the emission of gravitational waves. Global defects reach scaling mainly through long-range interactions and emission of Goldstone bosons [125]. A defect network in scaling produces an irreducible background of GWs emitted continuously around the horizon scale at every moment of the cosmic history. Its spectrum is predicted to be exactly scale-invariant for the modes that are emitted during radiation domination [115]. At the level of the power spectrum, this background mimics therefore the shape of the inflationary background due to quantum fluctuations. The irreducible emission of GWs from a defect network is however expected to be highly non-Gaussian. This is simply due to the fact that the source of the GWs is the (transverse-traceless part of the) energy-momentum of the network, and this is a function bilinear in the amplitude (modulo derivatives) of the fields that the cosmic defects are made of. Since the GW source is bilinear in field amplitudes, this implies automatically that any correlator of an odd number of tensor perturbations will be characterized by the correlation of an even product of fields. This is non-vanishing even if the fields were Gaussian. Thus, odd tensor correlation functions are non-vanishing, i.e. the GW background is not Gaussian. As the GWs are continuously emitted around the horizon scale at every moment, we cannot apply now the previous causal argument based on the superposition of many domains from the past.

Even though the shape of the power spectrum of the irreducible GW background from defects is well understood theoretically, its ultimate amplitude depends on the fine details of the so called *unequal-time-correlator* of the network's energy-momentum tensor. Unfortunately, this correlator that can only be obtained accurately from sufficiently fine lattice simulations of defect networks. It is therefore difficult to assess at this point whether this background can be detectable with LISA, much less whether its 3-point function can be measured. The GW signal can be however estimated analytically in a simplified case, known as the large N limit of a global phase transition due to the spontaneous symmetry breaking of $O(N)$ into $O(N-1)$. This kind of phase transition leads to the formation of so called "self-ordering scalar field" configurations, which correspond to non-topological defects (textures). The scale-invariant GW power spectrum due to the dynamics of such global defects has been estimated, in the limit $N \gg 1$, by Refs. [121,122], whereas the 3-point function (in the equilateral configuration) has been presented in Ref. [123]. Order of magnitude calculations in the large N limit, has lead to a GW bispectrum peaked in the equilateral configuration as [123]

$$k^6 \mathcal{B}(k,k,k) \sim C_{NL} (k^{3/2} \mathcal{P}_h(k))^2 \,, \qquad \text{with } C_{NL} \sim \frac{3.6}{\sqrt{N}} \,, \tag{87}$$

where $\mathcal{P}_h$ is the total power spectrum (summing over the two polarizations) and $N \gg 1$ is the number of

a signal or to get a superposition of signals, leading to what is called a popcorn-like noise [124]. These signals due to bursts represent therefore, in a sense, a temporal deviation from Gaussianity, that can be measured from the two-point function. However they do not correspond to the type of non-Gaussianity that we discuss in this paper, as they do not form a continuous stochastic background.

components of the symmetry-breaking field. Even though this is a rough estimate, it clearly indicates that we should expect a large departure from Gaussianity for the irreducible GW background from any defect network. A proper assessment of the ability of LISA to detect the power spectrum and bispectrum of this stochastic background, requires however further work; namely lattice simulations of defect networks with a large dynamical range.

Let us finally comment on *string gas cosmology* [126, 127] a string theory motivated early universe scenario, which does not involve a period of cosmological inflation. The model is based upon T-duality, making use of (fundamental) string oscillatory modes and winding modes. In this scenario, the universe may have started in a a quasi-static Hagedorn phase, during which thermal fluctuations of closed (fundamental) strings generate the density perturbations. The obtained spectrum of cosmological perturbations [128], and of GWs [129] are nearly scale invariant. The power spectrum of scalar metric fluctuations has a slight red tilt, while the spectrum of gravitational waves has a slight blue tilt. The string gas model has one free parameter and one free function, the former being the ratio of the string to the Planck length, and the latter the wavenumber dependence of the temperature. In this scenario, the spectrum of cosmological fluctuations may have large non-Gaussianities due to the thermal origin of the initial perturbations leading to strong three-point correlations [130]. Such thermal effects have been shown to be important for some inflationary models, such as *chain* inflation [131] or *warm* inflation [132]. In string gas cosmology, the non-Gaussianities of the spectrum of cosmological fluctuations depend linearly on the wavenumber, while the amplitude depends sensitively on the string scale. In slow-roll inflation, to leading order in perturbation theory, matter fluctuations do not couple to tensor ones, whereas in string gas cosmology matter fluctuations induce both scalar and tensor fluctuations. Hence, one may expect also non-Gaussianities in the tensor modes, for which the formalism discussed in the previous sections may be applicable.

6 Conclusions

In this work we studied the three-point correlation function of the SGWB expected to be measured by LISA, and we developed the formalism required for this analysis. The $3-$point correlation function is a key observable to gain information on the statistics of this background and crucial in order to study its departure from Gaussianity. This can be a crucial discriminant for a signal of cosmological origin, since the stochastic background due to a large number of uncorrelated astrophysical sources is Gaussian to a very high degree, due to the central limit theorem. The $3-$point correlator (also known as bispectrum), if present in the data, is a much richer observable than the standard $2-$point correlator (the power spectrum), due to several reasons. Firstly, this is due to the frequency of the three modes present in the correlator. The wave-vectors of the modes entering in the correlator must add up to zero, namely $\vec{k} + \vec{k}' = 0$ for the power spectrum, and $\vec{k} + \vec{k}' + \vec{k}'' = 0$ for the bispectrum. For a statistically isotropic SGWB, the correlators depend only on the magnitude of the wave-vectors, the wavenumbers, and not on the orientation. Therefore the power spectrum only depends on the signal wavenumber (*i.e.* $|\vec{k}| = |\vec{k}'|$), while the bispectrum depends on an overall scaling, and on two relative sizes. This last dependence is known as the "shape" of the bispectrum. Secondly, a larger number of combinations of LISA channels can be measured in the three-point signal (as opposed to the response functions for the power spectrum, which are identical for the two noise-orthogonal A and E LISA channels [18] and vanish for their cross-correlation). Thirdly, the planar nature of the instrument (together with the assumption of statistical isotropy) results in the insensitivity of the two-point function to the polarization of the two GW modes. This situation is ameliorated for the

three-point function, since more combinations of GW polarizations can be considered (see below).

In eq. (6) we provided a very general parametrization for the case of a mildly non-Gaussian SGWB. This ansatz is borrowed from the wide literature on the non-Gaussianity of the primordial density perturbations probed through the fluctuations of the CMB radiation. This gives rise to a bispectrum of rather general shape (namely, the dependence on the wavenumbers of the three GW involved in the correlation, and, ultimately, on the frequencies of the three measured signals), see eq. (12). Different cosmological mechanisms produce non-Gaussianity of different shapes, so that this study can potentially be a powerful discriminant between them. In Section 5 we provided a survey of several possibilities present in the literature.

In Section 3 we computed the various 3−point LISA response functions $\mathcal{R}^{OO'O''}_{\lambda\lambda;\lambda''}(k, k', k'')$ that, together with the GW correlation function $\langle h_\lambda(k)\, h_{\lambda'}(k')\, h_{\lambda''}(k'')\rangle$, provide the signal $\langle s_O s_{O'} s_{O''}\rangle$ measured by the different LISA channels (we study the response for all possible combinations of the A and E channels). We provided the formulae to compute the response functions for generic wavenumbers, and we then provided the explicit results for two cases of particular relevance (as they probe distinct physical mechanisms for the generation of non-Gaussianity): the equilateral configuration $k = k' = k''$ and the isosceles squeezed configuration $k \ll k' = k''$. As we already mentioned, the planarity of the instrument results in identities between different response functions, in the case of an isotropic SGWB. It is most immediate to discuss this in terms of circular polarizations, as they change into each other under a parity transformation. In the 2−point functions we have $\mathcal{R}^{OO'}_{LL} = \mathcal{R}^{OO'}_{RR}$ (where L and R stand, respectively, for the left handed and the right handed circular polarization), resulting effectively in an inability to probe a chiral GW signal. On the other hand, for the three-point function we have $\mathcal{R}^{OO'O''}_{LLL} = \mathcal{R}^{OO'O''}_{RRR}$, and $\mathcal{R}^{OO'O''}_{LLR} = \mathcal{R}^{OO'O''}_{RRL}$, but these two objects are different from each other. They also contribute differently to the A and E channels, so that by combining different $\langle s^3\rangle$ signals, one can hope to discriminate between a chiral and a non-chiral SGWB.

Moreover, in Section 4 we constructed the frequency-dependent estimator for the SGWB bispectrum that maximizes the signal-to-noise ratio in the measurement. As an example, we evaluated the general formula for the estimator for the specific case of a non-Gaussian signal narrowly localized at one given scale, $k = k' = k'' = k_*$.

To summarize, we have provided the complete formalism to compute the 3−point correlation function of the signal measured at LISA for any given theoretical SGWB 3−point correlator. This formalism can be readily extended to any other combination of GW interferometers, such as LIGO. Moreover, if the primordial bispectrum is amplified on a squeezed shape – hence coupling modes of different frequencies – we can use the three-point function to correlate signals from different experiments probing distinct frequency ranges, as LISA, LIGO, or PTA. This can allow us to 'break' the planarity condition of a single interferometer, and measure effects of parity violation also in small frequency ranges that cannot be probed by other means (see also the discussion in Ref. [7]). If non-vanishing, measurements of 3−point correlation functions can provide a wealth of information on different cosmological mechanisms, due to its dependence on the scale, the shape, and, possibly, the polarization of the SGWB. Even a null measurement can set limits on specific models that would be otherwise be unconstrained. We leave this study to future work.

Acknowledgments

We thank Raphael Flauger, Michele Liguori, Sabino Matarrese, and Germano Nardini for useful discussions. We thank the Mainz Institute for Theoretical Physics (MITP) for hosting the IV LISA

workshop, where this work has started. NB acknowledges partial financial support by ASI Grant No. 2016-24-H.0. The work of D.G.F was supported by the Swiss National Science Foundation. JGB thanks the Theory Department at CERN for their hospitality during his sabbatical year at CERN. His work is supported by the Research Project FPA2015-68048-C3-3-P (MINECO-FEDER), the Centro de Excelencia Severo Ochoa Program SEV-2016-0597, and the Salvador de Madariaga Program Ref. PRX17/00056. The work of Marco Peloso was supported in part by the DOE grant de-sc0011842 at the University of Minnesota. Mauro Pieroni acknowledges the support of the Spanish MINECO's Centro de Excelencia Severo Ochoa Program SEV-2016-0597. This project has received funding from the European Unions Horizon 2020 research and innovation programme under the Marie Skłodowska-Curie grant agreement No 713366. The work of Mairi Sakellariadou is supported in part by the Science and Technology Facility Council (STFC), UK, under the research grant ST/P000258/1. The work of Lorenzo Sorbo is partially supported by the US-NSF grant PHY-1520292. Gianmassimo Tasinato is partially funded by the STFC grant ST/P00055X/1.

A Construction and properties of polarization operators

Let us first of all reproduce for clarity the tensor decomposition given in Eq. (1),

$$h_{ab}(t,\vec{x}) = \int d^3k\, \mathrm{e}^{-2\pi i\,\vec{k}\cdot\vec{x}} \sum_\lambda e_{ab,\lambda}(\hat{k})\, h_\lambda(t,\vec{k}) \,, \tag{A1}$$

expressed in terms of an arbitrary polarization basis $e_{ab,\lambda}(\hat{k})$. A basis for the polarization operators often considered in the literature is the $\{+,\,\times\}$ basis. To define it, we express each $\hat{k}$ in the $\{\hat{e}_1,\hat{e}_2,\hat{e}_3\}$ basis[9] in standard polar coordinates

$$\hat{k} = (\sin\theta\,\cos\phi,\,\sin\theta\,\sin\phi,\,\cos\theta) \,, \tag{A2}$$

and then introduce the vectors

$$\hat{u} = (\sin\phi,\,-\cos\phi,\,0) \quad , \quad \hat{v} = \hat{k}\times\hat{u} = (\cos\theta\cos\phi, \cos\theta\sin\phi, -\sin\theta)\,. \tag{A3}$$

The set $\{\hat{k},\,\hat{u},\,\hat{v}\}$ forms an orthonormal basis. We note that $\hat{k}$ and $\hat{u}$ are odd under parity, while $\hat{v}$ is even. Out of these vectors, we define

$$e^{(+)}_{ab} = \frac{\hat{u}_a\hat{u}_b - \hat{v}_a\hat{v}_b}{\sqrt{2}} \quad , \quad e^{(\times)}_{ab} = \frac{\hat{u}_a\hat{v}_b + \hat{v}_a\hat{u}_b}{\sqrt{2}} \,. \tag{A4}$$

They are real, and they satisfy $e^{(+)}_{ab}e^{(+)}_{ab} = e^{(\times)}_{ab}e^{(\times)}_{ab} = 1$, $e^{(+)}_{ab}e^{(\times)}_{ab} = 0$. We also note that $e^{(+)}_{ab}$ is even under parity, while $e^{(\times)}_{ab}$ is odd.

The chiral polarization operators are then defined as

$$e^{(R)}_{ab} = \frac{e^{(+)}_{ab} + i\, e^{(\times)}_{ab}}{\sqrt{2}} \equiv e_{ab,+1} \quad , \quad e^{(L)}_{ab} = \frac{e^{(+)}_{ab} - i\, e^{(\times)}_{ab}}{\sqrt{2}} \equiv e_{ab,-1} \,, \tag{A5}$$

and they satisfy the properties (3) given in the main text.

Let us now note that in eq. (A1) [c.f. eq. (1)], after choosing a polarization tensor basis (either the $+,\times$ or L,R basis), the decomposition still depends, for each $\hat{k}$, on the choice of the vectors

[9] This is the basis where we first placed a single interferometric arm in the 'z-direction' $\hat{e}_3$.

$\{\hat{u},\hat{v}\}$. For a given GW mode propagating in the direction $\hat{k} = (\sin\theta\cos\phi, \sin\theta\sin\phi, \cos\theta)$, our choice of the orthonormal basis $\{\hat{u},\hat{v}\}$ in eq. (A3) was actually arbitrary (though as we will see soon, very convenient). Even though the conditions $\hat{k}\cdot\hat{u} = \hat{k}\cdot\hat{v} = 0$ and $\hat{v} = \hat{k}\times\hat{u}$ (or equivalently $\hat{u} = \hat{v}\times\hat{k}$) must always be satisfied by construction (in order for $\{\hat{u},\hat{v},\hat{k}\}$ to form an orthonormal triad), the orientation of the $\{\hat{u},\hat{v}\}$ vectors within the plane transverse to $\hat{k}$ is arbitrary. In particular, our canonical choice of $\{\hat{u},\hat{v}\}$ can be arbitrarily rotated by an angle α around their 'z-axis' $\hat{k}$, into a new system $\{\hat{u}(\alpha),\hat{v}(\alpha),\hat{k}\}$, where $\hat{u}(0)\equiv\hat{u}$, $\hat{v}(0)\equiv\hat{v}$, with $\{\hat{u},\hat{v}\}$ given by eq. (A3). This can be implemented explicitly by a rotation matrix around the axis $\hat{k}$ as

$$\begin{pmatrix}\hat{u}(\alpha)\\ \hat{v}(\alpha)\end{pmatrix} = R[\alpha]\cdot\begin{pmatrix}\hat{u}\\ \hat{v}\end{pmatrix}, \qquad R[\alpha]\equiv\begin{pmatrix}\cos\alpha & \sin\alpha\\ -\sin\alpha & \cos\alpha\end{pmatrix}. \tag{A6}$$

In the $\{\hat{e}_1,\hat{e}_2,\hat{e}_3\}$ basis, the new vectors read, by components,

$$\hat{u}(\alpha) = (\cos\alpha\sin\phi + \sin\alpha\cos\theta\cos\phi, -\cos\alpha\cos\phi + \sin\alpha\cos\theta\sin\phi, -\sin\alpha\sin\theta) \tag{A7}$$

$$\hat{v}(\alpha) = (-\sin\alpha\sin\phi + \cos\alpha\cos\theta\cos\phi, \sin\alpha\cos\phi + \cos\alpha\cos\theta\sin\phi, -\cos\alpha\sin\theta)\,, \tag{A8}$$

from where it can be verified, using basic trigonometric identities, that $|\hat{u}(\alpha)|^2 = |\hat{v}(\alpha)|^2 = 1$ and $\hat{u}(\alpha)\times\hat{v}(\alpha) = (\sin\theta\cos\phi, \sin\theta\sin\phi, \cos\theta)\equiv\hat{k}$, as it should. The rotated triad $\{\hat{u}(\alpha),\hat{v}(\alpha),\hat{k}\}$ form therefore an equally valid orthonormal basis from which to build up new $+,\times$ polarizations tensors as

$$e_{ij}^{(+)}(\alpha) = \frac{\hat{u}_i(\alpha)\hat{u}_j(\alpha) - \hat{v}_i(\alpha)\hat{v}_j(\alpha)}{\sqrt{2}}\ , \ e_{ij}^{(\times)}(\alpha) = \frac{\hat{u}_i(\alpha)\hat{v}_j(\alpha) + \hat{v}_i(\alpha)\hat{u}_j(\alpha)}{\sqrt{2}}\,, \tag{A9}$$

The expressions (A7), (A8) are however not particularly illuminating. Using rather the new components expressed as $\hat{u}_i(\alpha) = \cos\alpha\,\hat{u}_i + \sin\alpha\,\hat{v}_i$, $\hat{v}_i(\alpha) = -\sin\alpha\,\hat{u}_i + \cos\alpha\,\hat{v}_i$, for $i = 1,2,3$, we realize (again using basic trigonometric relations) that $e_{ij}^{(+)}(\alpha) = \cos\alpha\, e_{ij}^{(+)} + \sin\alpha\, e_{ij}^{(\times)}$ and $e_{ij}^{(\times)}(\alpha) = -\sin\alpha\, e_{ij}^{(\times)} + \cos\alpha\, e_{ij}^{(+)}$, i.e.

$$\begin{pmatrix}e_{ij}^{(+)}(\alpha)\\ e_{ij}^{(\times)}(\alpha)\end{pmatrix} = R[\alpha]\cdot\begin{pmatrix}e_{ij}^{(+)}\\ e_{ij}^{(\times)}\end{pmatrix}. \tag{A10}$$

Thus, we see that the $+,\times$ polarization tensors in the new rotated basis $\{\hat{u}(\alpha),\hat{v}(\alpha)\}$, transform identically – through a rotation matrix – as the new rotated basis , c.f. eq. (A6). This implies that if we were to express the GW in eq. (1) in terms of the new $\left\{e_{ij}^{(+)}(\alpha),\, e_{ij}^{(\times)}(\alpha)\right\}$ tensors, the tensor modes should be equally rotated as

$$\begin{pmatrix}h_+(\alpha)\\ h_\times(\alpha)\end{pmatrix} = R[\alpha]\cdot\begin{pmatrix}h_+\\ h_\times\end{pmatrix}. \tag{A11}$$

Defining now a set of chiral polarization tensors in the rotated basis,

$$e_{ij}^{(R)}(\alpha) = \frac{e_{ab}^{(+)}(\alpha) + i\, e_{ab}^{(\times)}(\alpha)}{\sqrt{2}} \equiv e_{ab,+1}(\alpha)\ , \ e_{ij}^{(L)}(\alpha) = \frac{e_{ab}^{(+)}(\alpha) - i\, e_{ab}^{(\times)}(\alpha)}{\sqrt{2}} \equiv e_{ab,-1}(\alpha)\,, \tag{A12}$$

leads immediately to realize that the new chiral polarization tensors, relate to the "old" ones expressed in terms of the canonical 'unrotated' basis $\{\hat{u},\hat{v}\}$, as

$$e_{ij,\pm1}(\alpha) = e^{\mp i2\alpha}\, e_{ij,\pm1}\,, \tag{A13}$$

where the chiral polarization tensors on the right hand side are those from eq. (A5), and on the left hand side those from eq. (A12). This implies that if we were to express the GW in eq. (1) in terms of the new $\left\{e_{ij}^{(R)}(\alpha),\, e_{ij}^{(L)}(\alpha)\right\}$ tensors, the tensor modes should equally be re-scaled by an opposite phase as in eq. (A13), i.e.

$$h_{\pm 1}[\alpha] = e^{\pm i2\alpha} h_{\pm 1}\,, \tag{A14}$$

where $_{+1}$ represents R polarization and $_{-1}$ represents L polarization.

These transformation rules are actually not surprising, as they simply reflect the spin-2 nature of the tensor field h_{ij} representing the GWs. Equations (A13), (A14) are actually quite relevant for our calculations, as they determine the complex phase of the response function we have calculated in Section 3. Let us first of all, recall that in the canonical basis [c.f. eq. (A3)] in which we have presented our results, a crucial property we used was the transformation rule presented in eq. (3) [see also the dicussion about the odd/even behaviour of $\hat{u}, \hat{v}$, and hence about $e_{ab}^{+,\times}$, above and below eq. (A4)]. The bispectra $\mathcal{B}(k_1, k_2, k_3)$ presented along the main text were always computed for a tensor basis obeying the property expressed in eq. (3), namely that under a "parity" tranformation $\vec{k} \longrightarrow -\vec{k}$, the chirality polarization tensors transform as $e_{ab,\lambda}(-\vec{k}) = e^{*}_{ab,\lambda}(\vec{k})$. That property is certainly true when the polarization tensors are computed in the canonical basis $\{\hat{u}, \hat{v}\}$ of eq. (A3). However, in light of eq. (A13), we now see that such relations are not universal: on the contrary, they are only verified by a very small subset of orthonormal basis $\{\hat{u}(\alpha), \hat{v}(\alpha)\}$. In particular, from eq. (A13), and using eq. (3), we deduce immediately that, in general, under a flip of momentum, the rotated basis of polarization tensors transform as

$$e_{ab,\pm}[\alpha](-\vec{k}) = e^{\mp i2\alpha} e^{*}_{ab,\pm}(\vec{k})\,. \tag{A15}$$

Of course, for $\alpha = 0$ we recover the result expressed in eq. (3) that that used in the main text, i.e. $e_{ab,\lambda}(-\vec{k}) = e^{*}_{ab,\lambda}(\vec{k})$. We see that this result also holds for $\alpha = \pi$, which is nothing else but the flip of the canonical vectors as $\hat{u} \longrightarrow -\hat{u}$, $\hat{v} \longrightarrow -\hat{v}$. For any angle α for which $\alpha \bmod(\pi) \neq 0$, the property $e_{ab,\lambda}(-\vec{k}) = e^{*}_{ab,\lambda}(\vec{k})$ will not hold. For instance for $\alpha = \pi/2$, this is equivalent to $\hat{u} \longrightarrow \hat{v}$ and $\hat{v} \longrightarrow -\hat{u}$, and hence it holds that $e_{ab,\lambda}(-\vec{k}) = -e^{*}_{ab,\lambda}(\vec{k})$. In general, the result of flipping the momentum will introduce a phase, as indicated in eq. (A15).

It is clear then that the choice of a 'rotated' vector basis other than the canonical one(s), will determine the complex phase of the polarization tensor via eq. (A13), and hence this will have necessarily an impact on the final expression of the 3-point response function eq. (38) that we have derived in Section 3. The reason is that $\mathcal{R}_{\lambda\lambda'\lambda''}$ is always proportional to three polarization tensors, schematically $\sim e^{\lambda}_{**} e^{\lambda'}_{**} e^{\lambda''}_{**}$. Denoting as $\mathcal{R}_{\lambda\lambda'\lambda''}[\alpha]$ the response functions calculated in a orthonormal vector basis rotated an angle α (around each $\vec{k}$) with respect the canonical basis $\{\hat{u}, \hat{v}\}$ defined in eq. (A3), we deduce immediately that the following relations must be true

$$\mathcal{R}_{RRR}[\alpha] = e^{-i6\alpha}\mathcal{R}_{RRR}[0]\,, \tag{A16}$$

$$\mathcal{R}_{LLL}[\alpha] = e^{+i6\alpha}\mathcal{R}_{LLL}[0]\,, \tag{A17}$$

$$\mathcal{R}_{LRR}[\alpha] = e^{-i2\alpha}\mathcal{R}_{LRR}[0]\,, \tag{A18}$$

$$\mathcal{R}_{RLL}[\alpha] = e^{+i2\alpha}\mathcal{R}_{RLL}[0]\,, \tag{A19}$$

where the response functions $\mathcal{R}_{\lambda\lambda'\lambda''}[0]$ on the right hand side should be identified with the response functions we presented in the main text. Actually, we see now that the discussion below eq. (38),

about the reality condition of our three-point response function, only applies to the case we presented in the main part of text, based on using the canonical base. In light of eqs. (A16)-(A19) we see that we can rather have pure imaginary or simply complex response functions, simply depending on the choice of the phase α.

In summary, we emphasize that the response functions presented in the main part of the text (see Figs. 3 and 5) were computed in the canonical basis (A3). If these results are to be applied to a bispectrum of any given model (see eq. (12)), special care must be taken to use the same basis or to apply the phase rotations as indicated in eqs. (A16)-(A19).

B Tensor three-point function at non-equal times

To provide the expressions for the 2-point and 3-point correlators, we introduce a standard Fourier space decomposition

$$\begin{aligned} h_{ij}\left(t,\,\vec{x}\right) &= \int d^3k \mathrm{e}^{-2\pi i\vec{k}\cdot\vec{x}} \sum_{\lambda} \mathrm{e}_{ij,\lambda}\left(\hat{k}\right) h_{\lambda}\left(t,\,\vec{k}\right) \\ &= \int d^3k \mathrm{e}^{-2\pi i\vec{k}\cdot\vec{x}} \sum_{\lambda} \mathrm{e}_{ij,\lambda}\left(\hat{k}\right) \left[\mathrm{e}^{2\pi ikt} h_{\lambda}\left(\vec{k}\right) + \mathrm{e}^{-2\pi ikt} h^{*}_{\lambda}\left(-\vec{k}\right)\right] , \end{aligned} \tag{B1}$$

assuming that $h_{\lambda}\left(\vec{k}\right)$ is a stochastic variable that satisfies

$$\left\langle h_{\lambda_1}\left(\vec{k}_1\right) h^{*}_{\lambda_2}\left(\vec{k}\right)\right\rangle = \frac{P_{\lambda_1}(k_1)}{8\pi\, k_1^3}\delta(\vec{k}_1-\vec{k}_2)\,\delta_{\lambda_1\lambda_2} , \tag{B2}$$

where statistical isotropy has been assumed, and where we allow for the possibility of a chiral GW background, $P_R\left(k\right) \neq P_L\left(k\right)$. Then the two-point function at non-equal times reads

$$\left\langle h_{\lambda_1}\left(t_1,\,\vec{k}_1\right) h_{\lambda_2}\left(t_2,\,\vec{k}_2\right)\right\rangle = \frac{P_{\lambda_1}\left(k_1\right)}{4\pi k_1^3}\delta_{\lambda_1\lambda_2}\,\delta^{(3)}\left(\vec{k}_1+\vec{k}_2\right)\,\cos\left[2\pi k_1\left(t_1-t_2\right)\right] . \tag{B3}$$

To compute the three-point function at non-equal times, recall our ansatz (6) for small departures from a Gaussian stochastic background,

$$\begin{aligned} h_{\lambda}\left(t,\,\vec{k}\right) = h_{\lambda,g}\left(t,\,\vec{k}\right) + \sum_{\lambda',\lambda''} f_{\mathrm{NL}}^{\lambda,\lambda',\lambda''} \int d^3p\, d^3q\, h_{\lambda',g}\left(t,\,\vec{p}\right)\, h_{\lambda'',g}\left(t,\,\vec{q}\right) \\ \times\,\delta^{(3)}\left(\vec{k}-\vec{p}-\vec{q}\right)\, K_{\lambda\lambda'\lambda''}\left(-\vec{p},\,-\vec{q}\right) , \end{aligned} \tag{B4}$$

with the properties of kernel function given in Eq. (7),

$$K_{\lambda\lambda'\lambda''}\left(-\vec{k}_1,\,-\vec{k}_2\right) = K_{\lambda\lambda'\lambda''}\left(k_1,\,k_2,\,\hat{k}_2\cdot\hat{k}_3\right) \equiv K_{\lambda\lambda'\lambda''}\left(k_1,\,k_2;\,k_3\right) , \tag{B5}$$

where $\vec{k}_3 = -\vec{k}_1 - \vec{k}_2$, and with a symmetry in the first two arguments, $K_{\lambda\lambda'\lambda''}\left(k_1,\,k_2;\,k_3\right) = K_{\lambda\lambda'\lambda''}\left(k_1,\,k_2;\,k_3\right)$. From the ansatz (B4), and the 2-point correlator (B3), one then obtains the unequal time 3−point correlation function

$$\left\langle h_{\lambda_1}\left(t_1,\,\vec{k}_1\right) h_{\lambda_2}\left(t_2,\,\vec{k}_2\right) h_{\lambda_3}\left(t_3,\,\vec{k}_3\right)\right\rangle = \frac{\delta^{(3)}\left(\vec{k}_1+\vec{k}_2+\vec{k}_3\right)}{8\pi^2}$$

$$\times \Bigg\{ f_{\rm NL}^{\lambda_1,\lambda_2,\lambda_3}\, K_{\lambda_1;\lambda_2,\lambda_3}\left(k_1; k_2, k_3\right) \frac{P_{\lambda_2}\left(k_2\right)}{k_2^3} \frac{P_{\lambda_3}\left(k_3\right)}{k_3^3} \cos\left[2\pi k_2\left(t_2-t_1\right)\right] \cos\left[2\pi k_3\left(t_3-t_1\right)\right]$$
$$+ f_{\rm NL}^{\lambda_2,\lambda_1,\lambda_3}\, K_{\lambda_2;\lambda_1,\lambda_3}\left(k_2; k_1, k_3\right) \frac{P_{\lambda_1}\left(k_1\right)}{k_1^3} \frac{P_{\lambda_3}\left(k_3\right)}{k_3^3} \cos\left[2\pi k_1\left(t_1-t_2\right)\right] \cos\left[2\pi k_3\left(t_3-t_2\right)\right]$$
$$+ f_{\rm NL}^{\lambda_3,\lambda_1,\lambda_2}\, K_{\lambda_3;\lambda_1,\lambda_2}\left(k_3; k_1, k_2\right) \frac{P_{\lambda_1}\left(k_1\right)}{k_1^3} \frac{P_{\lambda_2}\left(k_2\right)}{k_2^3} \cos\left[2\pi k_1\left(t_1-t_3\right)\right] \cos\left[2\pi k_2\left(t_2-t_3\right)\right] \Bigg\} . \tag{B6}$$

C Comparison with GW decomposition in the frequency basis

It is instructive to compare the GW decomposition (1) used in this paper with the decomposition in terms of positive and negative frequencies that is often encountered in the literature of the stochastic GW background [133]

$$h_{ab}\left(t, \vec{x}\right) = \int_{-\infty}^{+\infty} df \int d^2\hat{n} \sum_{\lambda} \mathrm{e}_{ab,\lambda}\left(\hat{n}\right) \mathrm{e}^{2\pi i f\left(t-\hat{n}\cdot\vec{x}\right)} h_{\lambda}\left(f, \hat{n}\right) , \tag{C1}$$

where we are considering left and right polarizations, and where the requirement of a real GW background is used to define the negative frequency field, $h_{\lambda}\left(-f, \hat{n}\right) = h^*_{-\lambda}\left(f, \hat{n}\right)$ (in the $\{+, \times\}$ basis, one has instead $h_{\sigma}\left(-f, \hat{n}\right) = h^*_{\sigma}\left(f, \hat{n}\right)$). Using this property, the decomposition (C1) can be rewritten as

$$\begin{aligned} h_{ab}\left(t, \vec{x}\right) &= \int_0^{+\infty} df \int d^2\hat{n} \sum_{\lambda} \mathrm{e}_{ab,\lambda}\left(\hat{n}\right) \left[\mathrm{e}^{2\pi i f\left(t-\hat{n}\cdot\vec{x}\right)} h_{\lambda}\left(f, \hat{n}\right) + \mathrm{e}^{-2\pi i f\left(t-\hat{n}\cdot\vec{x}\right)} h_{\lambda}\left(-f, \hat{n}\right)\right] \\ &= \int_0^{+\infty} df \int d^2\hat{n}\, \mathrm{e}^{-2\pi i f \hat{n}\cdot\vec{x}} \sum_{\lambda} \mathrm{e}_{ab,\lambda}\left(\hat{n}\right) \left[\mathrm{e}^{2\pi i f t}\, h_{\lambda}\left(f, \hat{n}\right) + \mathrm{e}^{-2\pi i f t}\, h^*_{\lambda}\left(f, -\hat{n}\right)\right] , \end{aligned} \tag{C2}$$

where we note that we also sent $\{\hat{n}, \lambda\} \to \{-\hat{n}, -\lambda\}$ in the second term of the second line. Comparing this with the first line of (1) allows to relate the operators in the two decompositions as

$$h_{\lambda}\left(f, \hat{n}\right) = k^2 \left[h_{\lambda}\left(\vec{k} = f\,\hat{n}\right) \theta\left(f\right) + h^*_{-\lambda}\left(\vec{k} = -f\,\hat{n}\right) \theta\left(-f\right)\right] . \tag{C3}$$

Using the relation between the two lines of (1) we can also relate the operator in (C1) to the full GW Fourier transform as

$$h_{\lambda}\left(f, \hat{n}\right) = \frac{\mathrm{e}^{-2\pi i f t}}{2} f^2 \left[h_{\mathrm{sign}\, f \times \lambda}\left(t, \vec{k} = f\hat{n}\right) - \frac{i}{2\pi f} \dot{h}_{\mathrm{sign}\, f \times \lambda}\left(t, \vec{k} = f\hat{n}\right)\right] , \tag{C4}$$

where dot denotes time differentiation.

We can use this relation to also relate correlators between modes in the two basis. For instance, for the 2−point correlator we have

$$\begin{aligned} \left\langle h_{\lambda}\left(f, \hat{n}\right) h_{\lambda'}\left(f', \hat{n}'\right)\right\rangle = \frac{\mathrm{e}^{-2\pi i\left(f t + f' t'\right)}}{4} f^2\, f'^2 \left[1 - \frac{i}{2\pi f} \frac{\partial}{\partial t}\right] \left[1 - \frac{i}{2\pi f'} \frac{\partial}{\partial t'}\right] \\ \times \left\langle h_{\mathrm{sign}\, f \times \lambda}\left(t, f\hat{n}\right)\, h_{\mathrm{sign}\, f' \times \lambda'}\left(t', f'\hat{n}'\right)\right\rangle . \end{aligned} \tag{C5}$$

Eq. (4) in the main text provides the equal time correlator in the Fourier basis. This is obtained from

$$\left\langle h_\lambda\left(\vec{k}\right) h_{\lambda'}\left(\vec{k}'\right)\right\rangle = 0 \ , \ \left\langle h_\lambda\left(\vec{k}\right) h^*_{\lambda'}\left(\vec{k}'\right)\right\rangle = \frac{P_\lambda(k)}{8\pi k^3}\,\delta_{\lambda\lambda'}\,\delta^{(3)}\left(\vec{k}-\vec{k}'\right) . \tag{C6}$$

These relations lead to the unequal time correlator

$$\left\langle h_\lambda\left(t,\vec{k}\right) h_{\lambda'}\left(t',\vec{k}'\right)\right\rangle = \cos\left[2\pi k\left(t-t'\right)\right]\,\frac{P_\lambda(k)}{4\pi k^3}\,\delta_{\lambda\lambda'}\,\delta^{(3)}\left(\vec{k}+\vec{k}'\right) , \tag{C7}$$

(which immediately reduces to (4) at equal times). Inserting this relation in (C5) leads to

$$\begin{aligned}
&\left\langle h_L(f,\hat{n})\, h_L\left(f',\hat{n}'\right)\right\rangle = \left\langle h_R(f,\hat{n})\, h_R\left(f',\hat{n}'\right)\right\rangle = 0 \, , \\
&\left\langle h_L(f,\hat{n})\, h_R\left(f',\hat{n}'\right)\right\rangle = \frac{P_L(f)\,\theta(f)+P_R(f')\,\theta(f')}{8\pi|f|}\,\delta\left(f+f'\right)\delta^{(2)}\left(\hat{n}-\hat{n}'\right) .
\end{aligned} \tag{C8}$$

As a check on our algebra, we verified that combining this result with the decomposition (C1) leads again to the equal-time real-space correlator (5).

D Technical calculations of Section 4.3

In this Appendix we provide some technical steps that were omitted in the computation of Section 4.3. Inserting the kernel of eq (66) relation into eqs. (49) and (55), we obtain

$$\begin{aligned}
S_s^{ijk}(f_1,f_2f_3) \;=\; & \frac{L^3\,f_{\rm NL}^{LLL}}{32\,\pi^2}\int\frac{dk_1}{k_1}\frac{dk_2}{k_2}\frac{dk_3}{k_3}\,k_1^2k_2^2k_3^2\,\mathcal{R}^{ijk}_{LLL}(k_1,k_2,k_3)\,{\rm e}^{-\frac{1}{2\sigma^2}\left[(k_1-k_*)^2+(k_2-k_*)^2+(k_3-k_*)^2\right]} \\
& \times\left\{\frac{P_L(k_2)}{k_2^3}\,\frac{P_L(k_3)}{k_3^3}\,\delta\left(k_2-|f_2|\right)\delta\left(k_3-|f_3|\right)+2\text{ permutations}\right\} .
\end{aligned} \tag{D1}$$

The curly bracket has three terms. In each term, two dk_i integrals are immediately performed thanks to the $\delta-$functions. The third integral is performed in the limit of narrow width of the bump, in which the functions multiplying the exponential term are evaluated at k_*. For instance, in the first term $k_1\,\mathcal{R}^{ink}_{LLL}(k_1,|f_2|,|f_3|)\,{\rm e}^{-\frac{(k_1-k_*)^2}{2\sigma^2}} \simeq k_*\,\mathcal{R}^{ink}_{LLL}(k_*,|f_2|,|f_3|)\,{\rm e}^{-\frac{(k_1-k_*)^2}{2\sigma^2}}$. The third integral is then also immediately done by extending it from $-\infty$ to ∞ (which is also appropriate in the narrow width approximation). We obtain

$$\begin{aligned}
S_s^{ijk}(f_1,f_2,f_3) \;\simeq\; & \frac{L^3\,f_{\rm NL}^{LLL}}{32\,\pi^2}\sqrt{2\pi}\,\sigma\,k_*\left\{\frac{P_L(|f_2|)}{f_2^2}\,\frac{P_L(|f_3|)}{f_3^2}\,{\rm e}^{-\frac{1}{2\sigma^2}\left[(|f_2|-k_*)^2+(|f_3|-k_*)^2\right]}\,\mathcal{R}^{ijk}_{LLL}(k_*,|f_2|,|f_3|)\right. \\
& \left.+2\text{ permutations}\right\} .
\end{aligned} \tag{D2}$$

We need to square this quantity, and insert it in (61). The mixed products between the three different terms in the curly bracket provide a negligible contribution to this result. Let us for instance discuss the product between the first and the second term. In the narrow peak approximation, the first term is mostly supported at $|f_2|=|f_3|=k_*$, while the second term at $|f_1|=|f_3|=k_*$. So the mixed product is supported only around the points where the magnitude of all the frequencies is equal to k_*. But this is incompatible with the $\delta-$function $\delta(f_1+f_2+f_3)$ present in (61).

Therefore, for the purpose of computing the signal to noise ratio, only the sum of the square of the three terms in the curly bracket is relevant. In this sum we also approximate all functions multiplying the exponential terms by their value at the center of the bump. This leads to

$$S_s^{ijk}\left(f_1,f_2,f_3\right)^2 \;\cong\; \left[\frac{L^3\, f_{\rm NL}^{LLL}}{32\,\pi^2}\,\sqrt{2\pi}\,\sigma\,\frac{P_L^2\left(k_*\right)}{k_*^3}\right]^2 \mathcal{R}_{LLL}^{ijk}\left(k_*,k_*,k_*\right)^2 \times\left\{ \mathrm{e}^{-\frac{1}{\sigma^2}\left[\left(|f_2|-k_*\right)^2+\left(|f_3|-k_*\right)^2\right]} + \mathrm{e}^{-\frac{1}{\sigma^2}\left[\left(|f_1|-k_*\right)^2+\left(|f_3|-k_*\right)^2\right]} + \mathrm{e}^{-\frac{1}{\sigma^2}\left[\left(|f_1|-k_*\right)^2+\left(|f_2|-k_*\right)^2\right]} \right\} . \tag{D3}$$

The three terms in the curly bracket provide the same contribution to the signal to noise ratio

$$\mathrm{SNR} \;\simeq\; \frac{L^3\, f_{\rm NL}^{LLL}}{32\,\pi^2}\,\sqrt{2\pi}\,\sigma\,\frac{P_L^2\left(k_*\right)}{k_*^3}\left[\frac{T}{6}\,\frac{1}{\left(4L^2\right)^3}\,\sum_{ijk}\mathcal{R}_{LLL}^{ijk}\left(k_*,k_*,k_*\right)^2 \times 3\int_{-\infty}^{+\infty}\frac{df_1}{P_n\left(|f_1|\right)}\int_{-\infty}^{+\infty}\frac{df_2}{P_n\left(|f_2|\right)}\,\mathrm{e}^{-\frac{\left(|f_2|-k_*\right)^2}{\sigma^2}}\int_{-\infty}^{+\infty}\frac{df_3}{P_n\left(|f_3|\right)}\,\mathrm{e}^{-\frac{\left(|f_3|-k_*\right)^2}{\sigma^2}}\,\delta\left(f_1+f_2+f_3\right)\right]^{1/2} . \tag{D4}$$

We perform the df_2 and the df_3 integrals in the narrow width limit. The second line of this expression then becomes

$$3\frac{\pi\sigma^2}{P_n^2\left(k_*\right)}\int_{-\infty}^{+\infty}\frac{df_1}{P_n\left(|f_1|\right)}\left[\delta\left(f_1-2k_*\right)+\delta\left(f_1\right)+\delta\left(f_1\right)+\delta\left(f_1+2k_*\right)\right] . \tag{D5}$$

The contribution proportional to $\delta\left(f_1\right)$ can be disregarded, since the noise diverges in that limit. This leads to eq. (67) written in the main text.

E Cosmological scaling of the non-linear parameter

The parameterization (6) of non-Gaussianity in terms of a nonlinear parameter is subject to the cosmological evolution, giving rise to the relation (10). When the momenta in the convolution have equal magnitude, we have a single rescaling, that can be roughly approximated as

$$f_{\rm NL} \simeq \frac{f_{\rm NL}^{\rm primordial}}{a_{k_*}} , \tag{E1}$$

where k_* is the magnitude of the momentum and a_{k_*} denotes the value of the scale factor when the modes re-entered the horizon. For GW generated after inflation inside the horizon, a_{k_*} denotes instead the value of the scale factor at the moment of the GW production. In this relation, the scale factor is normalized to one at the present time. In this appendix we estimate the value of a_{k_*} for both cases.

We start from GW generated during inflation. In this case, the modes re-enter the horizon during radiation domination. We can write

$$\frac{1}{a_{k_*}} \;=\; \frac{1}{a_{\rm eq}}\,\frac{a_{\rm eq}}{a_{k_*}} = \frac{1}{a_{\rm eq}}\,\sqrt{\frac{t_{\rm eq}}{t_*}} = \frac{1}{a_{\rm eq}}\,\frac{a_* H_*}{a_{\rm eq}\,H_{\rm eq}} , \tag{E2}$$

where we have used the fact that $a \propto t^{1/2}$ and $H \propto \frac{1}{t}$ during radiation domination. In this relation, the suffix 'eq' refers to the moment of matter-radiation equality, while the star denotes the moment at which the mode k_* re-enters the horizon.

At horizon re-entry, $a_* H_* = 2\pi k_*$, where the 2π is a consequence of the Fourier transform convention adopted in this work (see for instance eq. (1)). The Hubble rate scales as the square root of the energy density. At equality, the energy density was twice that of radiation, $\rho_{\rm eq} = 2 \times \rho_{\rm rad,eq} = 2 \times a_{\rm eq}^{-4}\, \rho_{\rm rad,0} = 2 \times a_{\rm eq}^{-4}\, \Omega_{\rm rad,0}\, \rho_0$, where ρ_0 is the present value of the energy density. Therefore,

$$\frac{1}{a_{k_*}} \;=\; \frac{2\pi k_*}{a_{\rm eq}^2}\, \frac{1}{H_0}\, \frac{1}{\sqrt{2\, a_{\rm eq}^{-4}\, \Omega_{\rm rad,0}}}\,. \tag{E3}$$

In scaling the energy density of radiation as a^{-4} we have disregarded the fact that massive neutrinos become non-relativistic, so we consistently evaluate the present fractional density in radiation as if neutrinos were massless, leading to $\Omega_{\rm rad,0} \simeq 4.18 \times 10^{-5} h^{-2}$. This leads to

$$\frac{1}{a_{k_*}} \;\simeq\; 2 \times 10^{17}\, \frac{k_*}{10^{-3}\,{\rm Hz}} \;\;,\;\; \text{production from inflation}\,. \tag{E4}$$

This corresponds to a temperature of $T \simeq \frac{T_0}{a_*} \sim 50\,{\rm TeV}$ (disregarding the variation of relativistic degrees of freedom).

Let us instead assume that the GW are produced inside the horizon, when the temperature of the universe was T_*. For convenience, we normalize the temperature at $100\,{\rm GeV}$. We then have (disregarding the variation of relativistic degrees of freedom for the purpose of our estimate)

$$\frac{1}{a_{k_*}} \sim \frac{T_*}{T_0} \simeq 4 \times 10^{14}\, \frac{T_*}{100\,{\rm GeV}} \;\;,\;\; \text{production inside horizon at temperature } T_*\,. \tag{E5}$$

References

[1] M. Maggiore, *Gravitational Waves. Vol. 1: Theory and Experiments*Oxford Master Series in Physics (Oxford University Press, 2007).

[2] M. Maggiore, *Gravitational Waves. Vol. 2: Astrophysics and Cosmology* (Oxford University Press, 2018).

[3] C. Caprini and D. G. Figueroa, 1801.04268.

[4] J. D. Romano and N. J. Cornish, Living Rev. Rel. **20**, 2 (2017), [1608.06889], 10.1007/s41114-017-0004-1.

[5] LISA, P. Amaro-Seoane *et al.*, 1702.00786.

[6] Planck, P. A. R. Ade *et al.*, Astron. Astrophys. **594**, A17 (2016), [1502.01592], 10.1051/0004-6361/201525836.

[7] T. L. Smith and R. Caldwell, Phys. Rev. **D95**, 044036 (2017), [1609.05901], 10.1103/PhysRevD.95.044036.

[8] D. S. Salopek and J. R. Bond, Phys. Rev. **D42**, 3936 (1990), 10.1103/PhysRevD.42.3936.

[9] A. Gangui, F. Lucchin, S. Matarrese and S. Mollerach, Astrophys. J. **430**, 447 (1994), [astro-ph/9312033], 10.1086/174421.

[10] E. Komatsu and D. N. Spergel, Phys. Rev. **D63**, 063002 (2001), [astro-ph/0005036], 10.1103/PhysRevD.63.063002.

[11] D. Babich, P. Creminelli and M. Zaldarriaga, JCAP **0408**, 009 (2004), [astro-ph/0405356], 10.1088/1475-7516/2004/08/009.

[12] J. M. Maldacena, JHEP **05**, 013 (2003), [astro-ph/0210603], 10.1088/1126-6708/2003/05/013.

[13] V. Acquaviva, N. Bartolo, S. Matarrese and A. Riotto, Nucl. Phys. **B667**, 119 (2003), [astro-ph/0209156], 10.1016/S0550-3213(03)00550-9.

[14] R. Scoccimarro, L. Hui, M. Manera and K. C. Chan, Phys. Rev. **D85**, 083002 (2012), [1108.5512], 10.1103/PhysRevD.85.083002.

[15] C. Wagner, L. Verde and L. Boubekeur, JCAP **1010**, 022 (2010), [1006.5793], 10.1088/1475-7516/2010/10/022.

[16] M. Liguori, S. Matarrese and L. Moscardini, Astrophys. J. **597**, 57 (2003), [astro-ph/0306248], 10.1086/378394.

[17] L. S. Finn, Phys. Rev. **D79**, 022002 (2009), [0810.4529], 10.1103/PhysRevD.79.022002.

[18] M. R. Adams and N. J. Cornish, Phys. Rev. **D82**, 022002 (2010), [1002.1291], 10.1103/PhysRevD.82.022002.

[19] N. J. Cornish, Phys. Rev. **D65**, 022004 (2002), [gr-qc/0106058], 10.1103/PhysRevD.65.022004.

[20] N. Cornish and T. Robson, 1803.01944.

[21] R. Namba, M. Peloso, M. Shiraishi, L. Sorbo and C. Unal, JCAP **1601**, 041 (2016), [1509.07521], 10.1088/1475-7516/2016/01/041.

[22] S. Kuroyanagi, T. Takahashi and S. Yokoyama, JCAP **1502**, 003 (2015), [1407.4785], 10.1088/1475-7516/2015/02/003.

[23] BICEP2, Keck Array, P. A. R. Ade *et al.*, Phys. Rev. Lett. **116**, 031302 (2016), [1510.09217], 10.1103/PhysRevLett.116.031302.

[24] Planck, P. A. R. Ade *et al.*, Astron. Astrophys. **594**, A20 (2016), [1502.02114], 10.1051/0004-6361/201525898.

[25] M. Hazumi *et al.*, Proc. SPIE Int. Soc. Opt. Eng. **8442**, 844219 (2012), 10.1117/12.926743.

[26] CORE, F. Finelli *et al.*, JCAP **1804**, 016 (2018), [1612.08270], 10.1088/1475-7516/2018/04/016.

[27] CMB-S4, K. N. Abazajian *et al.*, 1610.02743.

[28] J. M. Maldacena and G. L. Pimentel, JHEP **09**, 045 (2011), [1104.2846], 10.1007/JHEP09(2011)045.

[29] A. Agrawal, 1804.01481.

[30] X. Gao, T. Kobayashi, M. Yamaguchi and J. Yokoyama, Phys. Rev. Lett. **107**, 211301 (2011), [1108.3513], 10.1103/PhysRevLett.107.211301.

[31] J. Soda, H. Kodama and M. Nozawa, JHEP **08**, 067 (2011), [1106.3228], 10.1007/JHEP08(2011)067.

[32] M. Shiraishi, D. Nitta and S. Yokoyama, Prog. Theor. Phys. **126**, 937 (2011), [1108.0175], 10.1143/PTP.126.937.

[33] M. C. Guzzetti, N. Bartolo, M. Liguori and S. Matarrese, Riv. Nuovo Cim. **39**, 399 (2016), [1605.01615], 10.1393/ncr/i2016-10127-1.

[34] T. Kobayashi, M. Yamaguchi and J. Yokoyama, Prog. Theor. Phys. **126**, 511 (2011), [1105.5723], 10.1143/PTP.126.511.

[35] M. Zumalacarregui and J. Garcia-Bellido, Phys. Rev. **D89**, 064046 (2014), [1308.4685], 10.1103/PhysRevD.89.064046.

[36] J. Gleyzes, D. Langlois, F. Piazza and F. Vernizzi, Phys. Rev. Lett. **114**, 211101 (2015), [1404.6495], 10.1103/PhysRevLett.114.211101.

[37] D. Langlois and K. Noui, JCAP **1602**, 034 (2016), [1510.06930], 10.1088/1475-7516/2016/02/034.

[38] D. Langlois and K. Noui, JCAP **1607**, 016 (2016), [1512.06820], 10.1088/1475-7516/2016/07/016.

[39] M. Crisostomi, K. Koyama and G. Tasinato, JCAP **1604**, 044 (2016), [1602.03119], 10.1088/1475-7516/2016/04/044.

[40] J. Ben Achour *et al.*, JHEP **12**, 100 (2016), [1608.08135], 10.1007/JHEP12(2016)100.

[41] Y. Akita and T. Kobayashi, Phys. Rev. **D93**, 043519 (2016), [1512.01380], 10.1103/PhysRevD.93.043519.

[42] T. Noumi and M. Yamaguchi, 1403.6065.

[43] A. Lue, L.-M. Wang and M. Kamionkowski, Phys. Rev. Lett. **83**, 1506 (1999), [astro-ph/9812088], 10.1103/PhysRevLett.83.1506.

[44] R. Jackiw and S. Y. Pi, Phys. Rev. **D68**, 104012 (2003), [gr-qc/0308071], 10.1103/PhysRevD.68.104012.

[45] M. Crisostomi, K. Noui, C. Charmousis and D. Langlois, Phys. Rev. **D97**, 044034 (2018), [1710.04531], 10.1103/PhysRevD.97.044034.

[46] N. Bartolo and G. Orlando, JCAP **1707**, 034 (2017), [1706.04627], 10.1088/1475-7516/2017/07/034.

[47] N. Bartolo *et al.*, JCAP **1612**, 026 (2016), [1610.06481], 10.1088/1475-7516/2016/12/026.

[48] J. L. Cook and L. Sorbo, Phys. Rev. **D85**, 023534 (2012), [1109.0022], 10.1103/PhysRevD.86.069901, 10.1103/PhysRevD.85.023534.

[49] L. Senatore, E. Silverstein and M. Zaldarriaga, JCAP **1408**, 016 (2014), [1109.0542], 10.1088/1475-7516/2014/08/016.

[50] D. Carney, W. Fischler, E. D. Kovetz, D. Lorshbough and S. Paban, JHEP **11**, 042 (2012), [1209.3848], 10.1007/JHEP11(2012)042.

[51] M. Biagetti, M. Fasiello and A. Riotto, Phys. Rev. **D88**, 103518 (2013), [1305.7241], 10.1103/PhysRevD.88.103518.

[52] M. Biagetti, E. Dimastrogiovanni, M. Fasiello and M. Peloso, JCAP **1504**, 011 (2015), [1411.3029], 10.1088/1475-7516/2015/04/011.

[53] C. Goolsby-Cole and L. Sorbo, JCAP **1708**, 005 (2017), [1705.03755], 10.1088/1475-7516/2017/08/005.

[54] L. Sorbo, JCAP **1106**, 003 (2011), [1101.1525], 10.1088/1475-7516/2011/06/003.

[55] M. M. Anber and L. Sorbo, Phys. Rev. **D85**, 123537 (2012), [1203.5849], 10.1103/PhysRevD.85.123537.

[56] N. Barnaby and M. Peloso, Phys. Rev. Lett. **106**, 181301 (2011), [1011.1500], 10.1103/PhysRevLett.106.181301.

[57] N. Barnaby *et al.*, Phys. Rev. **D86**, 103508 (2012), [1206.6117], 10.1103/PhysRevD.86.103508.

[58] A. Maleknejad and M. M. Sheikh-Jabbari, Phys. Lett. **B723**, 224 (2013), [1102.1513], 10.1016/j.physletb.2013.05.001.

[59] E. Dimastrogiovanni and M. Peloso, Phys. Rev. **D87**, 103501 (2013), [1212.5184], 10.1103/PhysRevD.87.103501.

[60] P. Adshead, E. Martinec and M. Wyman, Phys. Rev. **D88**, 021302 (2013), [1301.2598], 10.1103/PhysRevD.88.021302.

[61] P. Adshead, E. Martinec and M. Wyman, JHEP **09**, 087 (2013), [1305.2930], 10.1007/JHEP09(2013)087.

[62] I. Obata, T. Miura and J. Soda, Phys. Rev. **D92**, 063516 (2015), [1412.7620], 10.1103/PhysRevD.95.109902, 10.1103/PhysRevD.92.063516.

[63] A. Maleknejad, JHEP **07**, 104 (2016), [1604.03327], 10.1007/JHEP07(2016)104.

[64] E. Dimastrogiovanni, M. Fasiello and T. Fujita, JCAP **1701**, 019 (2017), [1608.04216], 10.1088/1475-7516/2017/01/019.

[65] A. Agrawal, T. Fujita and E. Komatsu, 1707.03023.

[66] P. Adshead and E. I. Sfakianakis, JHEP **08**, 130 (2017), [1705.03024], 10.1007/JHEP08(2017)130.

[67] R. R. Caldwell and C. Devulder, Phys. Rev. **D97**, 023532 (2018), [1706.03765], 10.1103/PhysRevD.97.023532.

[68] A. Agrawal, T. Fujita and E. Komatsu, 1802.09284.

[69] J. R. Espinosa, D. Racco and A. Riotto, 1804.07732.

[70] M. Peloso, L. Sorbo and C. Unal, JCAP **1609**, 001 (2016), [1606.00459], 10.1088/1475-7516/2016/09/001.

[71] J. Garcia-Bellido, M. Peloso and C. Unal, JCAP **1612**, 031 (2016), [1610.03763], 10.1088/1475-7516/2016/12/031.

[72] M. Shiraishi, C. Hikage, R. Namba, T. Namikawa and M. Hazumi, Phys. Rev. **D94**, 043506 (2016), [1606.06082], 10.1103/PhysRevD.94.043506.

[73] B. Thorne *et al.*, Phys. Rev. **D97**, 043506 (2018), [1707.03240], 10.1103/PhysRevD.97.043506.

[74] S. Endlich, A. Nicolis and J. Wang, JCAP **1310**, 011 (2013), [1210.0569], 10.1088/1475-7516/2013/10/011.

[75] N. Bartolo, D. Cannone, A. Ricciardone and G. Tasinato, JCAP **1603**, 044 (2016), [1511.07414], 10.1088/1475-7516/2016/03/044.

[76] A. Ricciardone and G. Tasinato, Phys. Rev. **D96**, 023508 (2017), [1611.04516], 10.1103/PhysRevD.96.023508.

[77] A. Ricciardone and G. Tasinato, JCAP **1802**, 011 (2018), [1711.02635], 10.1088/1475-7516/2018/02/011.

[78] G. Domènech *et al.*, JCAP **1705**, 034 (2017), [1701.05554], 10.1088/1475-7516/2017/05/034.

[79] G. Ballesteros, D. Comelli and L. Pilo, Phys. Rev. **D94**, 124023 (2016), [1603.02956], 10.1103/PhysRevD.94.124023.

[80] D. Cannone, J.-O. Gong and G. Tasinato, JCAP **1508**, 003 (2015), [1505.05773], 10.1088/1475-7516/2015/08/003.

[81] C. Lin and L. Z. Labun, JHEP **03**, 128 (2016), [1501.07160], 10.1007/JHEP03(2016)128.

[82] D. Cannone, G. Tasinato and D. Wands, JCAP **1501**, 029 (2015), [1409.6568], 10.1088/1475-7516/2015/01/029.

[83] M. Akhshik, JCAP **1505**, 043 (2015), [1409.3004], 10.1088/1475-7516/2015/05/043.

[84] T. Takahashi and J. Soda, Phys. Rev. Lett. **102**, 231301 (2009), [0904.0554], 10.1103/PhysRevLett.102.231301.

[85] T. Zhu, W. Zhao, Y. Huang, A. Wang and Q. Wu, Phys. Rev. **D88**, 063508 (2013), [1305.0600], 10.1103/PhysRevD.88.063508.

[86] Y. Huang, A. Wang, R. Yousefi and T. Zhu, Phys. Rev. **D88**, 023523 (2013), [1304.1556], 10.1103/PhysRevD.88.023523.

[87] J. L. Cook and L. Sorbo, JCAP **1311**, 047 (2013), [1307.7077], 10.1088/1475-7516/2013/11/047.

[88] J. Garcia-Bellido, M. Peloso and C. Unal, JCAP **1709**, 013 (2017), [1707.02441], 10.1088/1475-7516/2017/09/013.

[89] M. Shiraishi, A. Ricciardone and S. Saga, JCAP **1311**, 051 (2013), [1308.6769], 10.1088/1475-7516/2013/11/051.

[90] M. Shiraishi, M. Liguori and J. R. Fergusson, JCAP **1501**, 007 (2015), [1409.0265], 10.1088/1475-7516/2015/01/007.

[91] R. Flauger, J. C. Hill and D. N. Spergel, JCAP **1408**, 039 (2014), [1405.7351], 10.1088/1475-7516/2014/08/039.

[92] U. Seljak and C. M. Hirata, Phys. Rev. **D69**, 043005 (2004), [astro-ph/0310163], 10.1103/PhysRevD.69.043005.

[93] P. D. Meerburg, J. Meyers, A. van Engelen and Y. Ali-Haïmoud, Phys. Rev. **D93**, 123511 (2016), [1603.02243], 10.1103/PhysRevD.93.123511.

[94] M. Shiraishi, M. Liguori and J. R. Fergusson, JCAP **1801**, 016 (2018), [1710.06778], 10.1088/1475-7516/2018/01/016.

[95] R. Easther and E. A. Lim, JCAP **0604**, 010 (2006), [astro-ph/0601617], 10.1088/1475-7516/2006/04/010.

[96] J. Garcia-Bellido and D. G. Figueroa, Phys. Rev. Lett. **98**, 061302 (2007), [astro-ph/0701014], 10.1103/PhysRevLett.98.061302.

[97] J. Garcia-Bellido, D. G. Figueroa and A. Sastre, Phys. Rev. **D77**, 043517 (2008), [0707.0839], 10.1103/PhysRevD.77.043517.

[98] J. F. Dufaux, A. Bergman, G. N. Felder, L. Kofman and J.-P. Uzan, Phys. Rev. **D76**, 123517 (2007), [0707.0875], 10.1103/PhysRevD.76.123517.

[99] J.-F. Dufaux, G. Felder, L. Kofman and O. Navros, JCAP **0903**, 001 (2009), [0812.2917], 10.1088/1475-7516/2009/03/001.

[100] J.-F. Dufaux, D. G. Figueroa and J. Garcia-Bellido, Phys. Rev. **D82**, 083518 (2010), [1006.0217], 10.1103/PhysRevD.82.083518.

[101] D. G. Figueroa and F. Torrenti, JCAP **1710**, 057 (2017), [1707.04533], 10.1088/1475-7516/2017/10/057.

[102] P. Adshead, J. T. Giblin and Z. J. Weiner, 1805.04550.

[103] M. Kamionkowski, A. Kosowsky and M. S. Turner, Phys. Rev. **D49**, 2837 (1994), [astro-ph/9310044], 10.1103/PhysRevD.49.2837.

[104] C. Caprini, R. Durrer and G. Servant, Phys. Rev. **D77**, 124015 (2008), [0711.2593], 10.1103/PhysRevD.77.124015.

[105] S. J. Huber and T. Konstandin, JCAP **0809**, 022 (2008), [0806.1828], 10.1088/1475-7516/2008/09/022.

[106] M. Hindmarsh, S. J. Huber, K. Rummukainen and D. J. Weir, Phys. Rev. Lett. **112**, 041301 (2014), [1304.2433], 10.1103/PhysRevLett.112.041301.

[107] M. Hindmarsh, S. J. Huber, K. Rummukainen and D. J. Weir, Phys. Rev. **D92**, 123009 (2015), [1504.03291], 10.1103/PhysRevD.92.123009.

[108] C. Caprini *et al.*, JCAP **1604**, 001 (2016), [1512.06239], 10.1088/1475-7516/2016/04/001.

[109] D. Cutting, M. Hindmarsh and D. J. Weir, 1802.05712.

[110] T. Vachaspati and A. Vilenkin, Phys. Rev. **D31**, 3052 (1985), 10.1103/PhysRevD.31.3052.

[111] M. Sakellariadou, Phys. Rev. **D42**, 354 (1990), 10.1103/PhysRevD.42.354, 10.1103/PhysRevD.43.4150.2.

[112] T. Damour and A. Vilenkin, Phys. Rev. Lett. **85**, 3761 (2000), [gr-qc/0004075], 10.1103/PhysRevLett.85.3761.

[113] T. Damour and A. Vilenkin, Phys. Rev. **D64**, 064008 (2001), [gr-qc/0104026], 10.1103/PhysRevD.64.064008.

[114] T. Damour and A. Vilenkin, Phys. Rev. **D71**, 063510 (2005), [hep-th/0410222], 10.1103/PhysRevD.71.063510.

[115] D. G. Figueroa, M. Hindmarsh and J. Urrestilla, Phys. Rev. Lett. **110**, 101302 (2013), [1212.5458], 10.1103/PhysRevLett.110.101302.

[116] J. J. Blanco-Pillado and K. D. Olum, Phys. Rev. **D96**, 104046 (2017), [1709.02693], 10.1103/PhysRevD.96.104046.

[117] D. G. Figueroa and T. Meriniemi, JHEP **10**, 101 (2013), [1306.6911], 10.1007/JHEP10(2013)101.

[118] J.-F. Dufaux, Phys. Rev. Lett. **103**, 041301 (2009), [0902.2574], 10.1103/PhysRevLett.103.041301.

[119] A. Tranberg, S. Tähtinen and D. J. Weir, JCAP **1804**, 012 (2018), [1706.02365], 10.1088/1475-7516/2018/04/012.

[120] L. M. Krauss, Phys. Lett. **B284**, 229 (1992), 10.1016/0370-2693(92)90425-4.

[121] K. Jones-Smith, L. M. Krauss and H. Mathur, Phys. Rev. Lett. **100**, 131302 (2008), [0712.0778], 10.1103/PhysRevLett.100.131302.

[122] E. Fenu, D. G. Figueroa, R. Durrer and J. Garcia-Bellido, JCAP **0910**, 005 (2009), [0908.0425], 10.1088/1475-7516/2009/10/005.

[123] P. Adshead and E. A. Lim, Phys. Rev. **D82**, 024023 (2010), [0912.1615], 10.1103/PhysRevD.82.024023.

[124] T. Regimbau, S. Giampanis, X. Siemens and V. Mandic, Phys. Rev. **D85**, 066001 (2012), [1111.6638], 10.1103/PhysRevD.85.066001, 10.1103/PhysRevD.85.069902.

[125] A. Vilenkin and E. P. S. Shellard, *Cosmic Strings and Other Topological Defects* (Cambridge University Press, 2000).

[126] R. H. Brandenberger and C. Vafa, Nucl. Phys. **B316**, 391 (1989), 10.1016/0550-3213(89)90037-0.

[127] M. Sakellariadou, Nucl. Phys. **B468**, 319 (1996), [hep-th/9511075], 10.1016/0550-3213(96)00123-X.

[128] A. Nayeri, R. H. Brandenberger and C. Vafa, Phys. Rev. Lett. **97**, 021302 (2006), [hep-th/0511140], 10.1103/PhysRevLett.97.021302.

[129] R. H. Brandenberger, A. Nayeri, S. P. Patil and C. Vafa, Phys. Rev. Lett. **98**, 231302 (2007), [hep-th/0604126], 10.1103/PhysRevLett.98.231302.

[130] B. Chen, Y. Wang, W. Xue and R. Brandenberger, The Universe **3**, 2 (2015), [0712.2477].

[131] B. Feldstein and B. Tweedie, JCAP **0704**, 020 (2007), [hep-ph/0611286], 10.1088/1475-7516/2007/04/020.

[132] A. Berera and L.-Z. Fang, Phys. Rev. Lett. **74**, 1912 (1995), [astro-ph/9501024], 10.1103/PhysRevLett.74.1912.

[133] B. Allen and J. D. Romano, Phys. Rev. **D59**, 102001 (1999), [gr-qc/9710117], 10.1103/PhysRevD.59.102001.